COGEAR

MODULE 1:

Earthquake-triggered landslides – spatial patterns and impacts

Del. No.: 1a.1.1

Author: Korup, O.

Swiss Federal Research Institutes WSL/SLF, Davos

January 31, 2010

CCES: Coupled Seismogenic Geohazards in Alpine Regions (COGEAR)

Module 1a – Report

Earthquake-triggered Landslides – Spatial Patterns and Impacts

---

Oliver Korup, PhD

Swiss Federal Research Institutes WSL/SLF, CH-7260 Davos, Switzerland[1]

31 January 2010

Executive Summary

This report gives an overview of recent quantitative studies that have highlighted specific spatial patterns of the occurrence of earthquake-triggered (or coseismic) landslides with respect to topographic, lithologic, and earthquake characteristics. It also deals with the subsequent geomorphic impacts that mainly arise from direct landslide contact with water bodies (i.e. landslide tsunami or seiches) and the delivery of coseismic landslide debris to the drainage network. Such off-site effects generally comprise, among others, the formation and failure of natural dams potentially giving rise to catastrophic outburst flows; elevated short-term fluvial and hyperconcentrated sediment yields; prolonged channel instability; and increased flood frequencies. Research along these lines has been mainly retrospective and empirical in nature, given the persistent difficulties of predicting the magnitude, timing, and location of landslide-triggering earthquakes. Yet the growing number of systematic studies on large and detailed inventories of coseismic landslides allows some general constraints on the patterns and possible consequences of these phenomena.

[1]Present Address: Institut für Erd- und Umweltwissenschaften, Universität Potsdam, D-14472 Potsdam, Germany, oliver.korup@geo.uni-potsdam.de

1. Background and Motivation

Earthquakes are among the most destructive geological processes on Earth, having caused an estimated minimum of 11 million fatalities in the past 4000 years (Fig. 1). The frequency of recorded destructive earthquakes has increased by three orders of magnitude over this period. This is due not to any significant change in seismicity, but rather to the increasingly detailed documentation of younger events and to the increase in human population, which has led to a higher exposure and damage potential for a given earthquake magnitude. Yet it has also long been recognised that loss of lives and damage attributed to earthquakes are to a significant fraction incurred by "secondary" earthquake effects such as tsunami, landslides, liquefaction, and fire rather than strong ground motion alone (Marano et al., 2010).

Therefore, the use of the term “secondary hazards” to characterise these effects is potentially misleading, given that any of subsequent process cascades may incur the highest fraction of total damage eventually. Earthquake-triggered (also termed coseismic) landslides are a particularly important process in this context. They represent the initial stage of earthquake-induced erosion and the first step in the sediment cascade, i.e. the downslope and downstream transfer of eroded soil and rock. Landslides involve the mobilisation of significant amounts of bedrock and superficial loose material, which is to be released from hillslopes and gradually transported downslope into river (and/or glacier) systems, which ultimately contribute to translating and dispersing large amounts of seimsically-induced sediment.

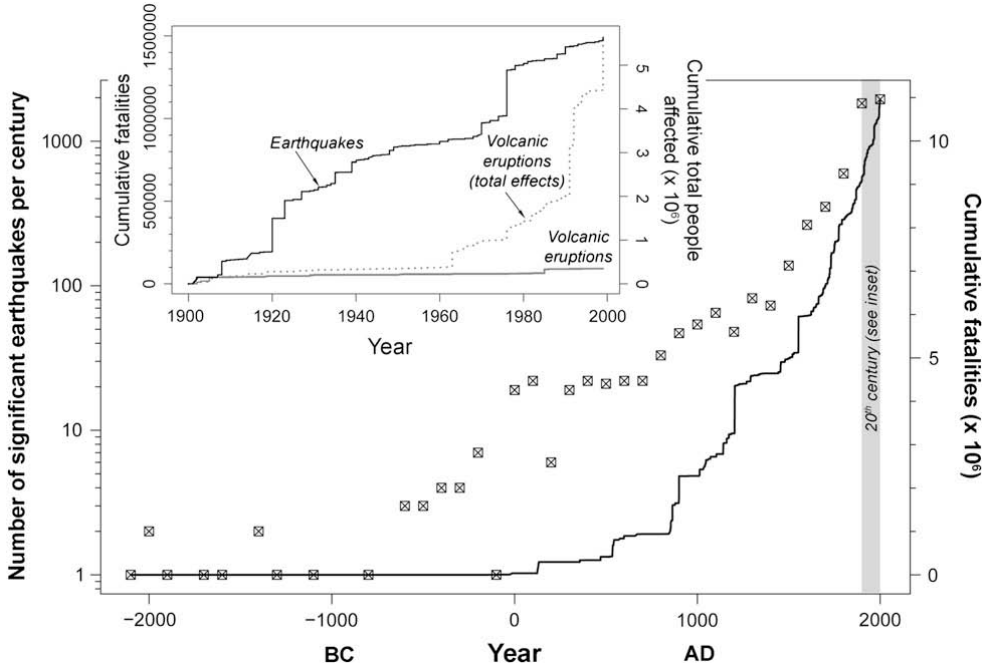

Fig. 1. Number of significant earthquakes per century for the past 4000 years (crossed squares), and the cumulative minimum number of associated fatalities (black line; data obtained from the National Geophysics Data Center,

http://www.ngdc.noaa.gov). Nearly 6000 earthquakes during this period have claimed at least 11 million lives. All events recorded here caused at least US$1 million damage, claimed more than 10 lives, had a magnitude >7.5 or Mercalli Intensity >X, or triggered a tsunami. Inset shows cumulative fatalities caused by 2522 earthquakes during the 20th century compared to those caused by 491 volcanic eruptions (Witham, 2005); the total number of people affected by these eruptions is also shown (after Korup and Clague, 2009).

Earthquakes are among the main triggers of landslides, which are defined here as the downward and outward movement of slope-forming materials under the influence of gravity, and in most cases also water (e.g. Cruden and Varnes, 1996). It is generally understood that horizontal (and in fewer cases vertical) ground acceleration resulting from seismic shaking exert additional transient shear stresses and increases to ambient porewater pressures through cyclic gravitational loading, thus negatively affecting slope stability (e.g. Sidle and Ochiai, 2006). Earthquakes can also serve as preparatory factors (or causes) of landslides. For example, repeated seismic hanging-wall shattering in reverse and thrust faults can contribute to weakening rock-mass strength through fragmentation. Moreover, the resulting creation of joints and pore spaces for groundwater may promote increased weathering and geochemical alteration of the source rock.

Overall, research on earthquake-triggered landslides has generally less progressed than that on rainfall-triggered landslides, mainly owing to a less clearly defined understanding of the contribution of seismic shaking to decreasing slope stability (Sidle and Ochiai, 2006). Moreover, earthquake-triggered landslides appear to be less frequent than those triggered by prolonged rainfall, leaving fewer opportunities to study the phenomenon in real time. Together with the general limitations of prediction the magnitude, location, and timing of large, landslide-triggering earthquakes, this has necessitated a strong retrospective and empirical approach to research on coseismic slope instability, with a strong focus on the analysis of past events (for a detailed review of the historic development of research see Keefer, 2002).

2. Research on earthquake-triggered landslides

The literature on earthquake-triggered landslides is extensive and continuously growing (Keefer, 2002). Research on earthquake-triggered landslides can be roughly divided into three avenues, i.e. studies that

(a) systematically document the distribution and characteristics of earthquake-triggered landslides and their geomorphic effects following historic events (e.g. Keefer, 1984;

1994; 1999; 2002; Pearce and Watson, 1986; Keefer and Manson, 1998; Barnard et al., 2001; Bommer and Rodriguéz, 2002; Di et al., 2010);

(b) model or otherwise quantitatively evaluate the susceptibility to earthquake-triggered slope instability (e.g. Jisbon et al., 2000; Bourdeau and Havenith, 2008; Lee et al., 2008; Miles and Keefer, 2009; Saygili and Rathje, 2009); and

(c) infer the intensity and/or timing of prehistoric earthquakes from characteristics of preserved landslide deposits or associated geomorphic evidence (e.g. Schuster et al., 1992; Crozier et al., 1995; Jibson, 1996; Bull and Brandon, 1998; Carrara and O'Neill, 2003; Beck, 2009).

This report mainly deals with the first avenue of research, and compiles findings on the spatial patterns of earthquake-induced landslides with respect to topography, lithology, and earthquake characteristics as well as their subsequent to river systems in terms of triggering further potentially adverse processes or altering the erosional and sedimentary budget. Nevertheless, a comprehensive study of the broad and rapidly growing literature body on earthquake-triggered landslides and their impacts is well beyond the scope of this report. Therefore, the objective of this report is to provide a broad overview on recent and necessarily selected advances in the field that have focused on systematically analysing earthquake-triggered landslides and their geomorphic impact in mountainous terrain.

3. Patterns of coseismic landslides

Systematic studies of earthquake-triggered landslides typically comprise analyses of size distributions and spatial patterns with respect to distance from the earthquake epicentre or ruptured master faults, hillslope inclination and position, and major lithologic units. In general, documented spatial patterns of earthquake-triggered landslides do reveal some systematic distribution with respect to these controls, though local variations may be considerable. Hence, in order to be representative, these analyses depend on as complete as possible landslide inventories (e.g. Rodriguéz et al., 1999; Bommer and Rodriguéz, 2002; Keefer, 2002; Malamud et al., 2004), which in turn rely on adequate remote sensing data sources for detection. These sources mainly comprise air photos, high-resolution satellite imagery, synthetic aperture radar (dinSAR), and LiDAR data (e.g. Guzzetti et al., 2009). All these methods have the potential for providing rapid quantitative assessments of landslide occurrence, especially in heavily damaged or barely accessible areas.

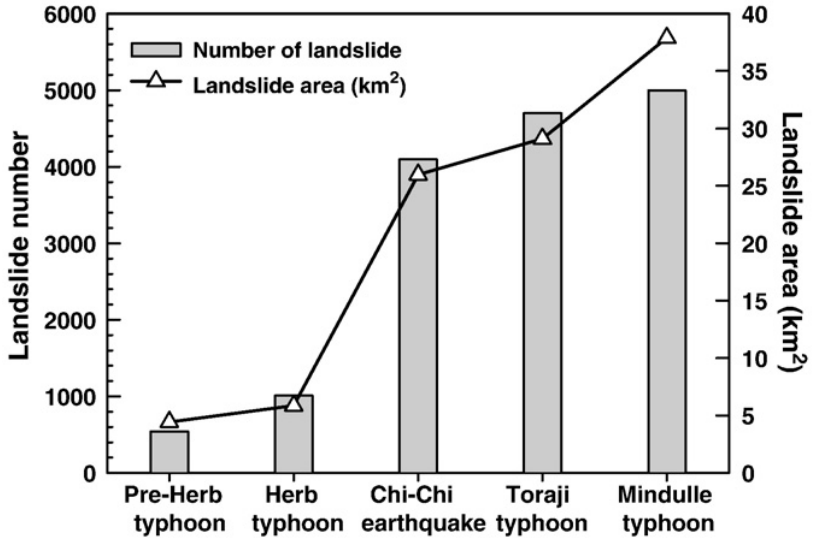

Fig. 2. Number of landslides in the Tachia catchment, Taiwan, following several regional landsliding episodes (after Chuang et al., 2009).

It is generally understood that earthquakes instantaneously increase the spatial abundance of landslides in a given area, expressed either as landslide density, i.e. the number of slope failures per unit study area [km^{-2}] or the fraction of landslide-affected terrain [%], often by an order of magnitude (Fig. 2). For example, two of the best studied recent earthquakes, i.e. the 2008 Wenchuan earthquake, China, and the 1999 Chi-Chi earthquake, Taiwan, had triggered >10,000 and ~22,000 landslides (Di et al., 2010). However, up to 50,000 landslides and more have been estimated to be the result of individual historic earthquakes (Keefer, 1999). Such values must remain first-order estimates essentially, particularly where hillslopes have been fully cleared by coseismic landslides, thus precluding any reliable distinction between individual failures. The same problem applies to hillslopes where anthropogenic modification is pronounced or natural revegation of hillslopes is rapid, where dense vegetation may cover smaller slope failures, or where earthquakes concur with or are followed by heavy rain causing further landslides. For example, during and in the wake of both the Chi-Chi and Wenchuan earthquakes, slope failures had stripped many hillslopes completely bare of any vegetation cover, thus making it intractable to discern individual failure scars, let alone landslide numbers (Fig. 3). Estimates of landside density further depend on the minimum size of detectable landslides, which is largely defined by the resolution of the remote sensing data as well as land-cover characteristics.

Fig. 3. Extremely steep slopes that were completely stripped of their vegetation as well as surficial soil and sediment cover by coseismic landslides of the 1999 Chi-Chi earthquake, central Taiwan, soon after the earthquake (left, October 1999), and largely revegetated nearly six years later (August 2005; after Lin et al., 2006). Despite these striking effects of earthquake-induced slope stability, it remains intractable to map the size and contribution of individual landslides.

However, estimates are possible for affected areas that have retained some vegetation or otherwise undisturbed surface cover for reference. Depending on the size and accessibility of study area, as well as the resolution of the remote sensing data used, average landslide frequencies ranging from 0.25 to 15 km^{-2} have been reported (Barnard et al., 2001; and Sato et al., 2007; respectively). For example, Yin et al. (2010) obtained a landslide density estimate of 13 km^{-2} for the epicentre region of the 2008 Wenchuan earthquake, based on the analysis of 1-m resolution digital orthophotos. These estimated peak values fall short of reaching rainstorm-triggered landslide densities, which in small (>10 km^2) catchments may be as high as 480 km^{-2} (Crozier, 2005), i.e. an order of magnitude higher. Indeed, Crozier (2005) lists at least eight rainfall-triggered regional landsliding episodes that have achieved nominally higher landslide densities than those recorded after earthquakes. Moreover, values of landslide density in small (<1 km^2) study catchments subjected to intensive agricultural use in Nepal may soar up to (though spatially very focused) peaks of 1800 km^{-2} (Thapa and Paudel, 2002).

Such estimates clearly depend on the size distribution of landslides, and higher densities are often correlated with lower median landslide sizes. Therefore, it is often more useful to quantify earthquake effects in terms of fraction of terrain affected by landslides. Reported values tend to be more reliable where remote sensing data allow clear distinction between pre- and post-earthquake conditions (e.g. Di et al., 2010; Fig. 4). Such differences are especially striking in areas of dense natural vegetation cover, which allow either manual or automated extraction of bare denuded areas that stand out because of a high spectral contrast. For example, Lin et al. (2006) proposed to use the normalised difference vegetation index (NDVI) for automatically extracting landslide-affected areas following the 1999 Chi-Chi

earthquake in a study area of central Taiwan. Based on a number of studies from detailed landslide inventories reported values of the fraction of terrain affected by coseismic landsliding range from 0.5% to 76%, depending on the extent of the study area and the distance to the epicentre (e.g. Keefer, 1999). In contrast, it is interesting to note that the majority of reported values for the fraction of terrain affected by rainstorm-triggered slope failures remain below 40%.

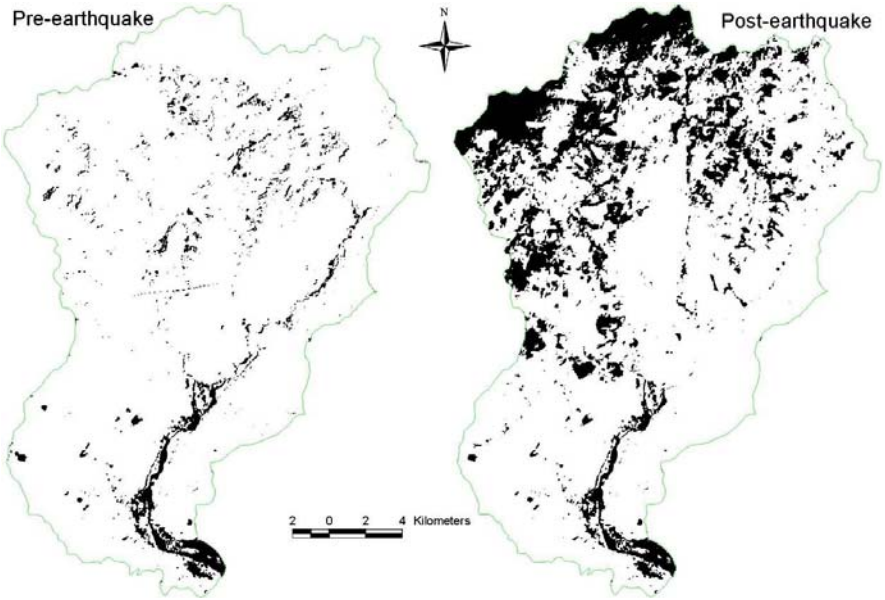

Fig. 4. Post-seismic five-fold increase in bare areas (defined as having vegetation cover <15%) due to coseismic landsliding during the 2008 Wenchuan earthquake in a study catchment near Wenchuan. Vegetation changes were based on landcover attributes obtained by Beijing-1 Microsatellite data at 35-m resolution. Overall fraction of terrain affected by coseismic landslides is estimated at 19% (after Di et al., 2010).

Keefer (1999) has been pioneering the systematic compilation and analysis of inventories of earthquake-triggered landslides, and proposed empirical curves on the basis of relationships between the total number and maximum area to be affected by landslides in relation to earthquake magnitude. He showed that both measures scale nonlinearly with earthquake magnitude (Fig. 5, Fig. 6). A similar nonlinear relationship with earthquake magnitude is observed for the maximum distance from the epicentre at which earthquake-triggered landslides have been identified. From these historical observations it follows that, depending on earthquake magnitude, areas between several to several hundreds of thousands of km^2 may be affected by coseismic slope instability. The minimum magnitude, based on empirical data from the United States, to trigger noticeable landsliding is M ~4, whereas the potential area to be affected by coseismic landsliding may be as high as 500,000 km^2 during magnitudes of M = 9.2 (Keefer, 1984). Importantly, such empirical relationships may differ somewhat between the regions they have been derived for (Keefer, 2002).

Such empirical approaches generally provide useful, though rough, estimates of the overall impact to be expected from a given earthquake magnitude, assuming that the data help constrain maximum envelope curves. However, recent strong earthquakes have triggered significantly lower numbers of landslides than those expected from Fig. 5. For example, the 2002 *M* = 7.9 Denali earthquake that mainly struck the mountainous glaciated terrain of Alaska, had triggered not only considerably fewer landslides than expected, but also focused their occurrence to a very narrow zone along the ruptured faults (Jibson et al., 2006). This highlights the limited applicability of such empirical relationships in terms of predicting the average rather than the maximum extent of coseismic slope instability.

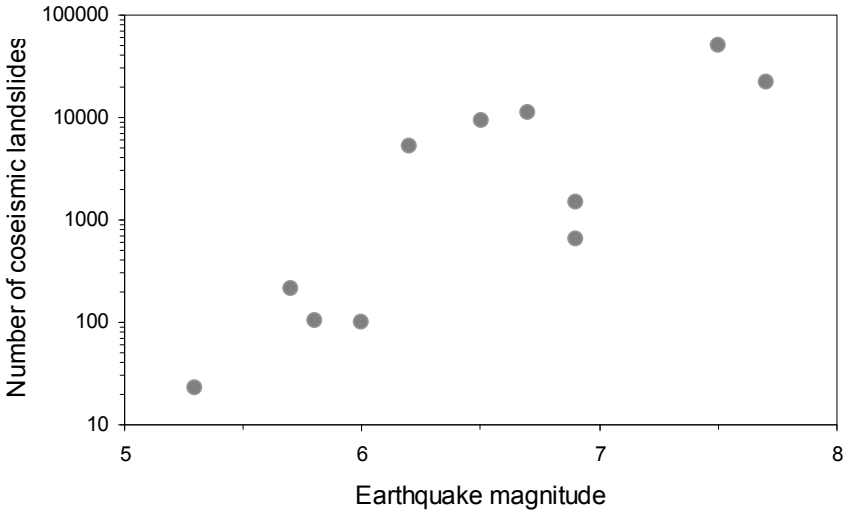

Fig. 5. Relation between total number of reported landslides and earthquake magnitude for earthquakes with comprehensive, i.e. statistically robust, inventories of landslides (data from Keefer, 2002).

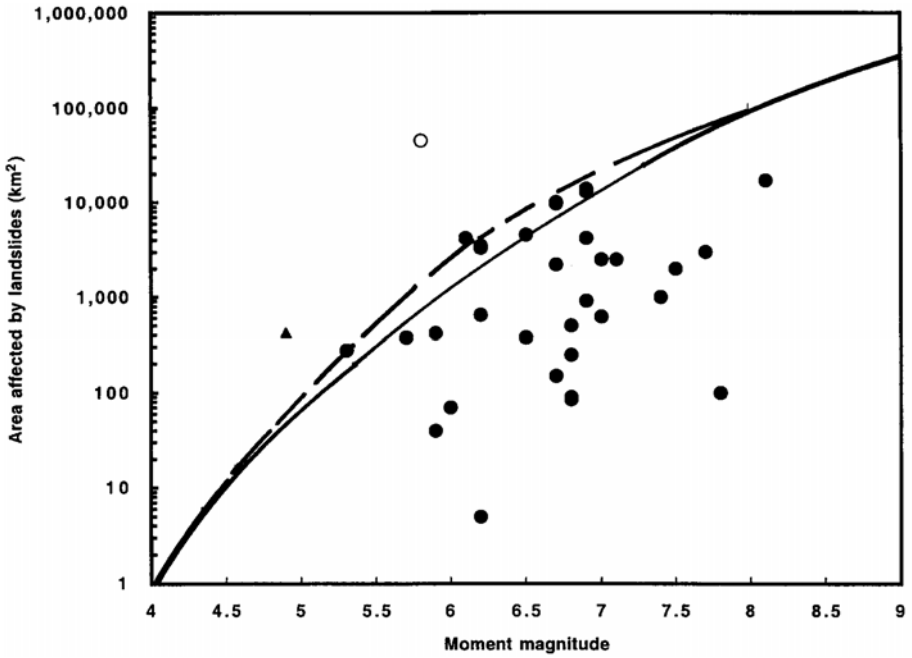

Fig. 6. Relations between area affected by landslides and earthquake moment magnitude (after Keefer, 2002). Circles are data from earthquakes discussed by Rodriguéz et al. (1999), plotted using moment magnitude (*M*); open circle is 1988 Saguenay, Quebec earthquake. Solid line is upper bound of Keefer (1984). Dashed line is upper bound of Rodriguéz et al. (1999). Triangle is datum from 1963 Peria, New Zealand, earthquake, for which area exceeds upper bounds, plotted using Richter local magnitude (ML), from Hancox et al. (2002); after Keefer (2002).

Comprehensive, i.e. statistically robust, landslide inventories are a basis for assessing the overall effects of earthquakes in terms of denudation, approximated as the spatially averaged amount of geologically instantaneous landscape surface lowering. In order to do so, the recorded individual landslide (planform or footprint) areas must be converted to landslide volumes. The 1950 M = 8.6 Assam earthquake, India, has so far been associated with the highest total volume of coseismic landslide sediment, i.e. an estimated 4.7×10^9 m^3. Keefer (1999) has shown that this and other estimated total volumes of coseismic landslides are nonlinearly correlated with earthquake magnitude. This is not surprising given that such estimates are based on empirical estimates of landslide volume-area scaling that are derived from limited field data (e.g. Malamud et al., 2004), or more pragmatically, by simply assuming a mean failure depth that is used to convert landslide areas into volumes (Fig. 7).

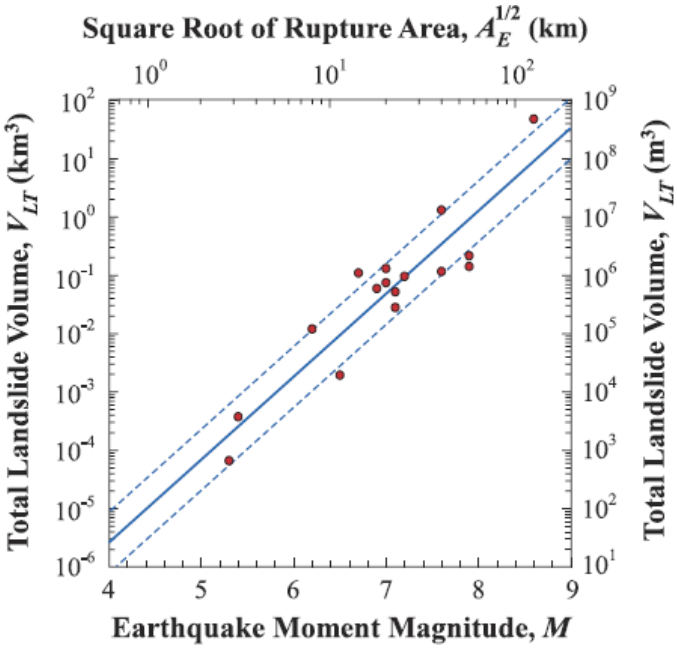

Fig. 7. Estimated total volume of landslides V_{LT} triggered by an earthquake as a function of earthquake moment magnitude M, and square root of equivalent rupture area $A_E^{0.5}$. Circles are volumes of landslides triggered by 16 earthquakes for which landslide volumes were estimated. Solid line is least-square best-fit straight line to the data; dashed lines give the standard deviations of the data with respect to the best fit (after Malamud et al., 2004).

However, Larsen et al. (2010) have shown that such global estimates may be prone to substantial errors, and caution against the straightforward application of empirical landslide volume-area scaling relationships for denudation estimates especially outside the study areas they were initially derived for. Specifically, they demonstrated that, despite the robustness of landslide size statistics, over- or underestimates of the total volume of landslides mobilized during earthquakes (and rainstorms) crucially depends on the choice of volume-are scaling exponents, as minute numerical differences may easily yield errors of the order of 100% or more (Fig. 8).

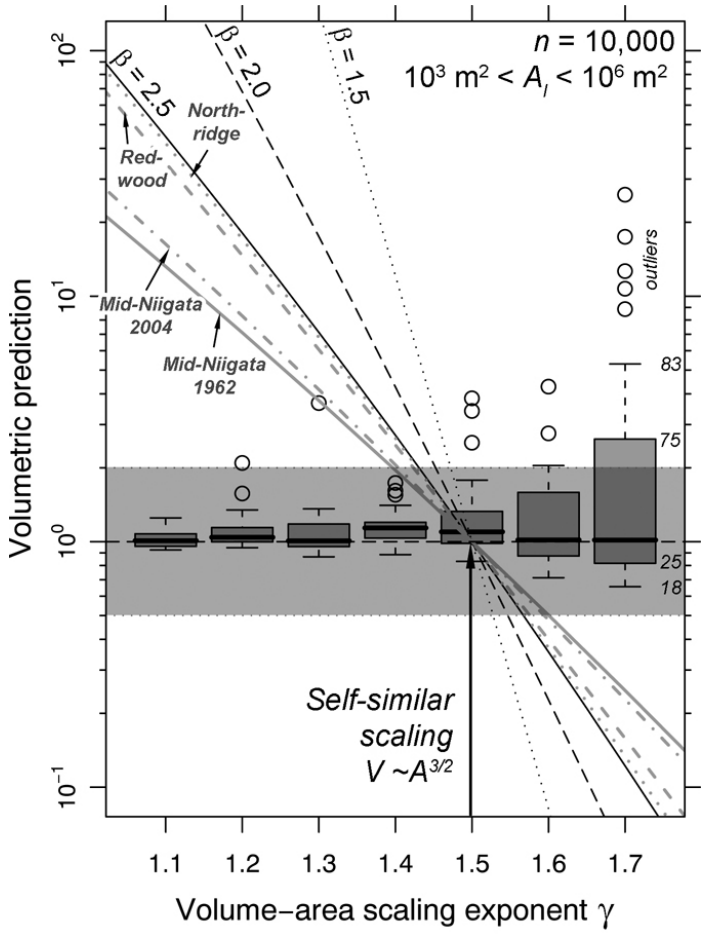

Fig. 8. Effect of empirical landslide volume-area scaling exponent *γ* on predicted total landslide volume (V_T). The total volumetric prediction is expressed as the ratio $V_T(\gamma=1.5)/V_T(\gamma)$ for three synthetic power-law distributed inventories (gray lines) and four empirical landslide inventories (black lines) of landslide area *A*, including the Northridge, USA, and Niigata, Japan, earthquakes. Gray shaded area encompasses factor of 2 under-/over-estimates. Boxes and whiskers depict ranges of volumetric prediction for 30 randomly-generated inventories of *A* for a fixed *γ*. Volumetric estimates from any two inventories with the same size range and scaling parameters generally vary by less than a factor of two, with the variance of the error increasing with *γ*, which is generally smaller than errors introduced by even small differences in *γ*. Synthetic power-law distributed landslide inventories (*n* = 10,000 each) have pre-defined range of non-cumulative area-frequency scaling exponents (*ß* = 1.5, 2.0, and 2.5) and landslide areas (10^3 m^2 < *A*l < 10^6 m^2), and encompass most published inventories (after Larsen et al., 2010).

A number of studies have further shown that the spatial distribution of coseismic landslides is not random, and many researchers have reported systematic patterns of landslide occurrence as a function of distance to the epicentre, slope gradient, slope position, and rock type (e.g. Keefer, 2002; Meunier et al., 2007). In planform view, a particularly strong erosional signal is that the landslide density declines nonlinearly with distance from the epicentre (Fig. 9). However, this pattern may be dissolved by significant differences in lithology and/or anthropogenic slope modification (e.g. Pearce and O'Loughlin, 1985; Keefer et al., 2006; Owen et al., 2008; Kamp et al., 2010). Yet the close spatial affinity of the majority of landslides to peak areas of strong ground motion along the ruptured faults has been documented in several independent studies. Moreover, analyses of the 2005 Kashmir

(Pakistan), the 2008 Wenchuan (China), and the 2008 Iwate-Miyagi Nairiku (Japan) earthquakes have demonstrated a significant over-abundance of landslides in the hanging walls of ruptured thrust faults (Sato et al., 2007; Yin et al., 2010; and Yagi et al., 2009, respectively) with respect to the foot walls. Exceptions seem to state this rule, as Yin et al. (2010) noted that the relationship between the number of landslides and the distance to the hanging wall of the rupture Wenchuan fault exhibited a more linear trend than that of the number of landslides with respect to the footwall of the fault.

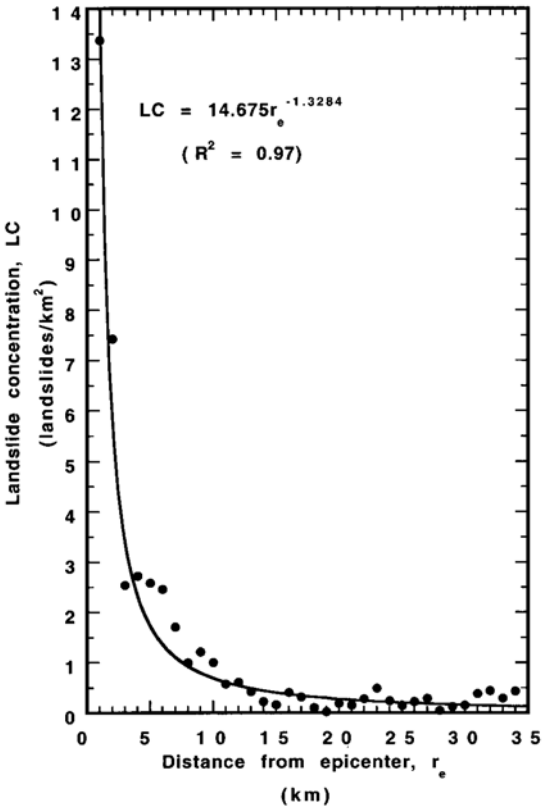

Fig. 9. Relation between landslide density [km^{-2}] and epicentral distance for landslides in the southern Santa Cruz Mountains triggered by the 1989 Loma Prieta, California, earthquake. Such a nonlinear decrease in landslide density away from the epicentre or master fault is an often observed phenomenon (after Keefer, 2002).

Another often observed characteristic that is of important consequence for landslide susceptibility studies and hazard zonings is that the majority of earthquake-triggered landslides predominantly detach from upper hillslope portions, i.e. close to ridges and interfluves. This effect is often attributed to topographic amplification of seismic ground shaking near ridges and interfluves. Lin et al. (2008b) quantitatively explored and confirmed this notion, finding that coseismic landslides preferentially attacked upper hillslope portions. Recent systematic analyses of large landslide inventories indicate that this pattern contrasts with spatial patterns derived from inventories of rainfall-triggered landslides, where slope failures tend to be more uniformly distributed with respect to hillslope position and distance from the drainage network (Fig. 10; Meunier et al., 2008).

Furthermore, the aspect of hillslopes and major landforms seems to modulate the local amplification of seismic signals (Del Gaudio and Wasowski, 2007). Earthquake-triggered landslides have often affected convex hillslopes where dynamic effects of seismic loading are more pronounced, whereas rainfall-triggered landslides preferentially occur in concave landscape elements, which tend to collect surface and groundwater (Sidle and Ochiai, 2006). In some cases, detachment of coseismic landslides also appears to preferentially occur on steeper slopes, as opposed to rainfall-triggered failures (Yamagishi and Iwahashi, 2007). Although there seems to be consensus that steeper hillslopes are more susceptible to coseismic landslides, few studies provided background information about the affected region's overall topography, so that it remains difficult to filter out whether the occurrence of earthquake-triggered landslides not simply mimics the distribution of slope inclinations in a given area.

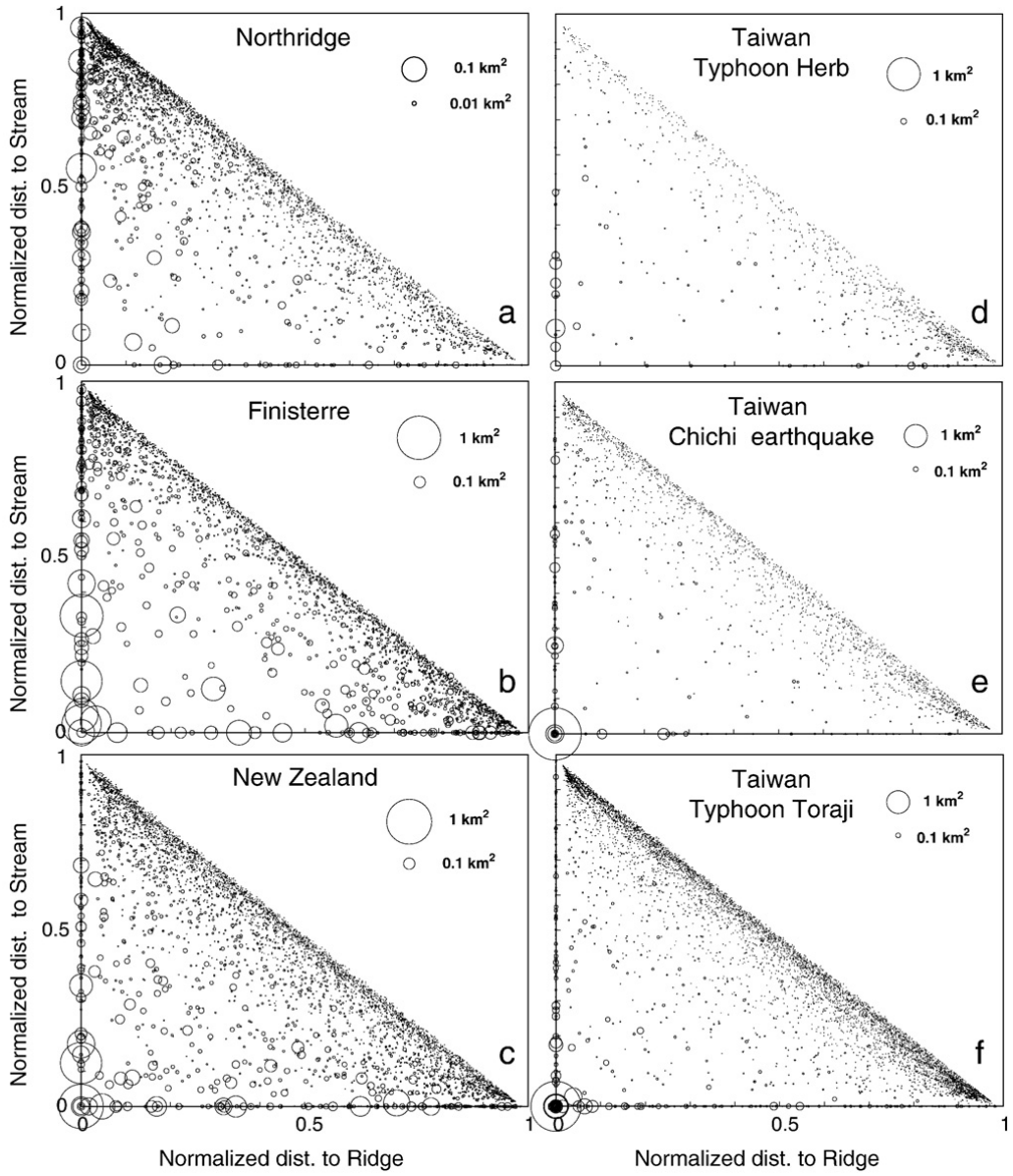

Fig. 10. Location of landslides with respect to ridge crest and stream. Distances from the landslide crown to the nearest ridge and from the lowest point on the landslide lobe to the nearest stream have been measured along the line of steepest descent, and normalized for the total length of the slope on which the landslide is located. The size (surface area) of the landslide is indicated with a circle of variable diameter. Landslides triggered by the Northridge earthquake (a) cluster around ridge crests. Landslides triggered by the 1993 earthquakes in the Finisterre Mountains (b) cluster at ridge crests and near the base of slopes. Rainfall-induced landslides in the western Southern Alps, NewZealand (c) are uniformly distributed. In central west Taiwan, landslides caused by typhoon Herb in 1996 (d) are clustered near streams, while the 1999 Chi-Chi Earthquake (e) triggered a significant number of landslides near ridge crests. The fingerprint of this shift toward the top of the slopes is still visible in the distribution of landslides triggered by typhoon Toraji in 2001) (f) (after Meunier et al., 2008).

4. Types of coseismic landslides

Judging from a number of landslide inventories, the most prominent and abundant type of earthquake-triggered landslides are shallow (<2 m), disrupted slope failures (Keefer, 2002).

These failures predominantly mobilise soil and debris, although smaller rock-slope failures have also been reported (e.g. Owen et al., 2008). However, there are only limited empirical relationships between landslide type and earthquake magnitude, and earthquakes of various magnitudes have reportedly triggered any possible type of landslide (Keefer, 2002; Sidle and Ochiai, 2006). Keefer (1984) found from the analysis of shaking intensity data from numerous earthquakes and their associated landslide occurrence several systematic relationships also between the type of landslide, earthquake magnitude, and the distance between a given landslide and the epicentre. Based on empirical data from the United States, the minimum earthquake magnitude for triggering rock falls, rock slides, and disrupted soil slides was M ~4. Rotational and blocky soil failures did occur at magnitudes ≥4.5, whereas lateral spreads, debris flows, subaquaeous failures, rotational and translational rock slides, and earthflows required higher magnitudes (≥5) to be triggered.

Empirical evidence further suggests that for a given earthquake magnitude, disrupted landslides may occur at larger distances from the epicentre than coherent landslides; this difference is particularly pronounced for smaller earthquakes (Keefer, 1999). Accordingly, the energy released during strong earthquakes is sufficient to trigger very large (10^6 m^3) catastrophic long-runout landslides. Keefer (1999) reports that in mountainous terrain large catastrophic rock avalanches (Fig. 11) have occurred at earthquake magnitudes ≥6. The largest historic and presumably earthquake-triggered (M = 7.4) rock-slope failure is the Usoi landslide, Tajikistan, which occurred in 1911. The rockslide entrained ~2.2 × 10^9 m^3 and continues to form the highest (~600 m) natural intact landslide dam in the world, impounding >60-km long Lake Sarez (Schuster and Alford, 2004). It is also the largest earthquake-triggered landslide to have occurred in the 20th century. Although several similarly sized, i.e. >10^9 m^3, catastrophic slope failures have been documented they have been either triggered by volcanic eruptions or detached without any noticeable triggers.

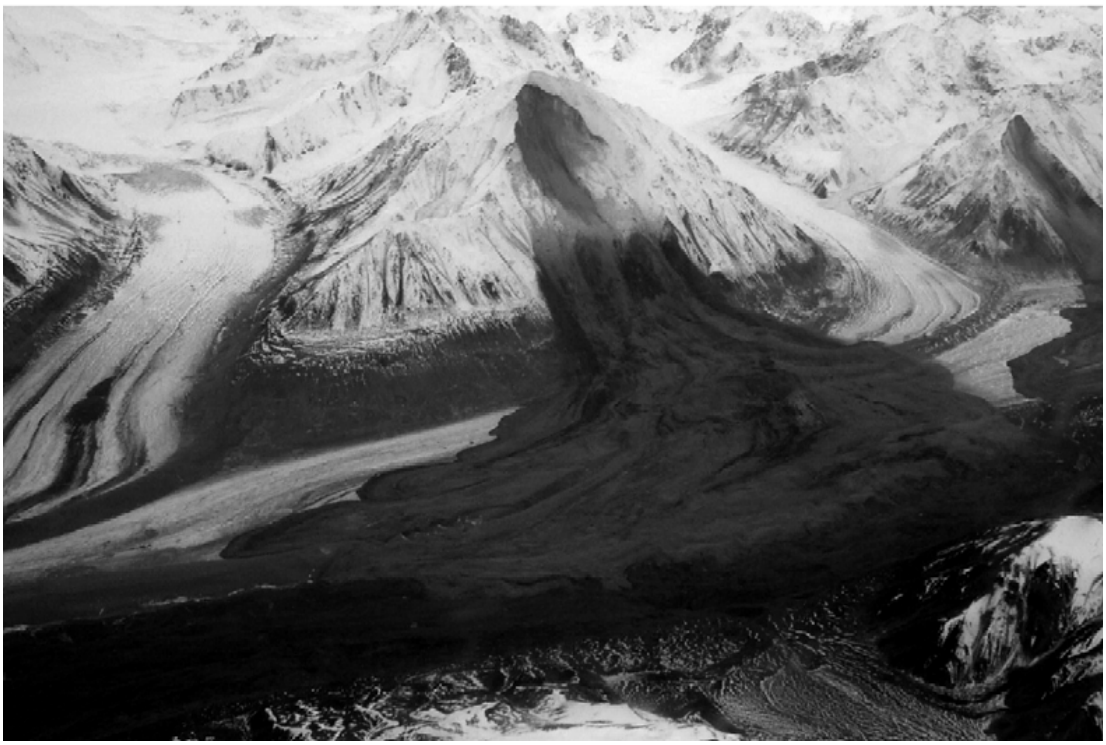

Fig. 11. Eastern Black Rapids rock avalanche, which ran out onto the Black Rapids Glacier, was triggered during *M* = 7.9 Denali earthquake, Alaska, 3 November 2002. This is the sort of catastrophic rock-slope failure to be expected for *M* >6 earthquakes in both formerly or presently glaciated mountainous terrain that provides sufficient topographic relief and slope steepness (after Jibson et al., 2006).

In glaciated terrain, earthquake-triggered ice and rock avalanches may fall into proglacial or otherwise naturally dammed lakes, thus causing displacement waves that may lead to dam overtopping and subsequent catastrophic failure of the dam (e.g. Schuster and Alford, 2004; Hubbard et al., 2005; Korup and Tweed, 2007). Also known as "aluviones" in South America, such earthquake-triggered process cascades are exemplified by the catastrophic and complex mass movement that detached from the peak of Nevado Huascaran, Peruvian Andes, in the wake of a M_s = 7.8 subduction earthquake (for a recent reassessment of the sequence of events see Evans et al., 2009a). The event started off as a rock fall containing substantial amounts of glacier ice and entrained significant amounts of snow and glacial deposits en route. The mass movement then transformed into a highly mobile debris flow that obliterated the town of Yungay, killing thousands of inhabitants, before sweeping further along the Rio Santa for several kilometres (Fig. 12, Fig. 13).

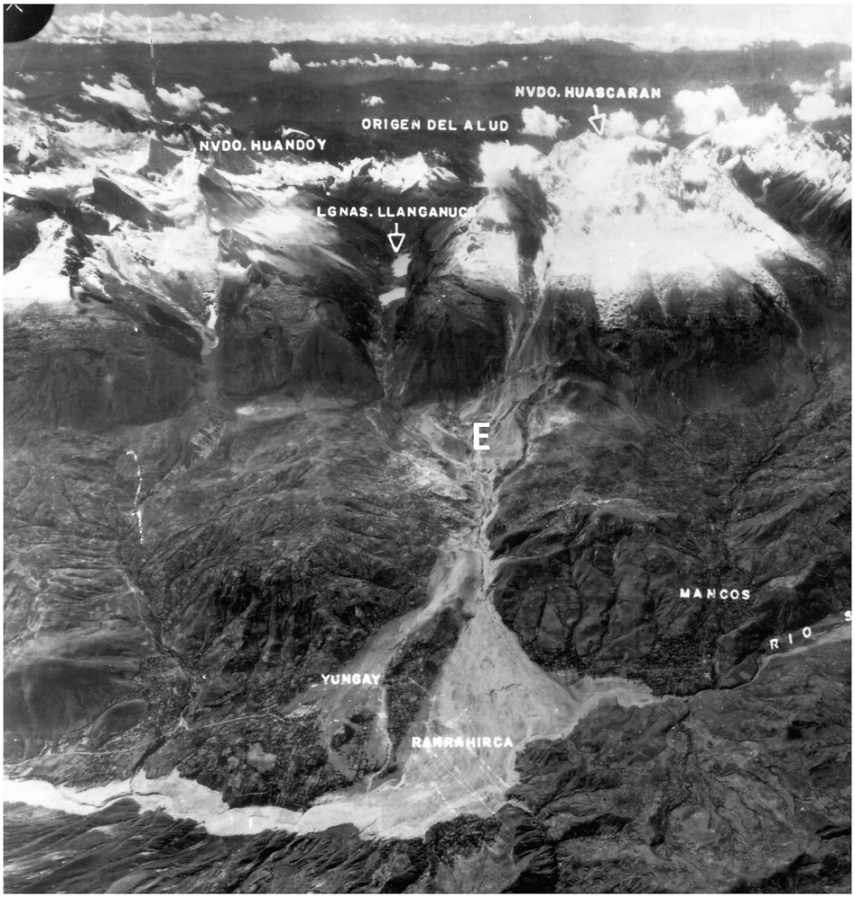

Fig. 12. Oblique aerial view to the east of the May 31, 1970 Huascarán event showing source, path, devastation of Yungay and the Ranrahirca fan, and beginning of downstream distal debris flow/debris flood following the Rio Santa off to the left. The extensive area of entrainment is seen below the terminal moraine system of Glacier 511 (E). Also visible is the peak of Huandoy, the source of an ice/rock fall triggered by the 1725 earthquake which generated a debris flow that led to the destruction of the town of Ancash. (Photograph and annotation; Servicío Aerofotografíco Nacional de Perú; June 13, 1970; after Evans et al., 2009a).

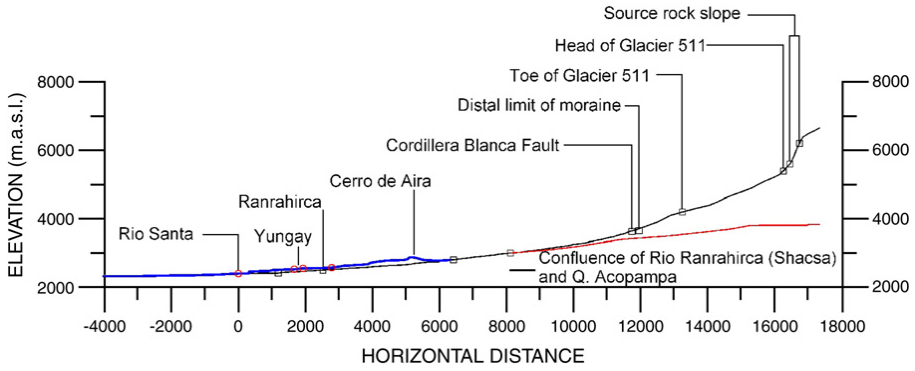

Fig. 13. Topographic profile of 1970 Huascarán event constructed from Department of Ancash 1:25,000 topographic map. Blue line is the profile of the Yungay Lobe and its continuation into the Rio Santa (after Evans et al., 2009a).

In contrast, where mountainous terrain sustains thick loess cover, earthquakes may trigger extremely mobile and potentially highly destructive loess flows that may originate on hillslopes with moderate to low inclinations, and readily interfere with the drainage network, causing ephemeral natural dams (<15°; Zhang and Wang, 2007). For example, Evans et al.

(2009b) have reconstructed that exceptionally large and long-runout rock fall/loess flows triggered by the 1949 Khait earthquake, Tajikistan, moved at average travel angles of as low as 2° (Fig. 14).

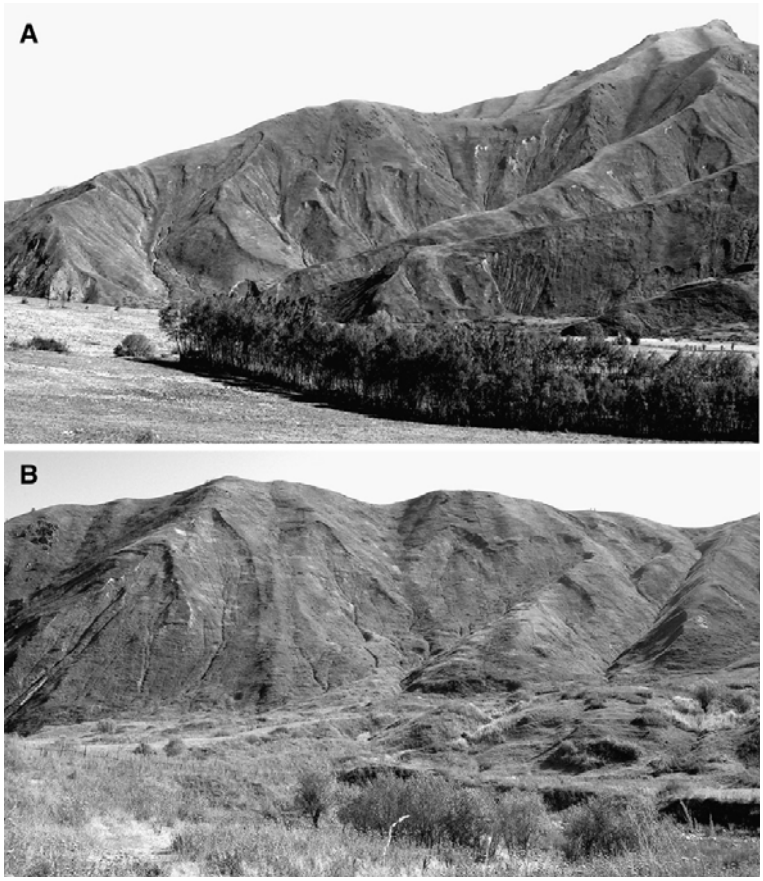

Fig. 14. Scars of loess flowslides on steep tributary slopes of the Yasman River, on the south side of the Yasman valley, as observed in 2006. The surface of the Yasman valley flow is visible in the foreground in both A and B. Downstream is to the left (after Evans et al., 2009b).

The strikingly obvious effects of catastrophic landslides triggered by earthquakes mask the difficulty of quantifying the spatial extent and potential consequences of non-catastrophic landslides related to seismic ground shaking. In addition to thousands of landslides, the 2005 Kashmir earthquake produced a number of conspicuous tension cracks that were interpreted to reflect the initial stages of slow-moving deep-seated landsliding with potential catastrophic termination (Bulmer et al., 2007). Despite initially high deformation rates no significant landslides seem to have been spawned from these cracks as yet. Tseng et al. (2009) applied particle image velocimetry to aerial orthophotos to quantify differential surface deformation associated with the creeping and potentially deep-seated Hongtsaiping landslide, central Taiwan. There, surface deformation was most pronounced in the days following the 1999 M_w = 7.6 Chi-Chi earthquake. This study site is only ~2.5 km away from the detachment area of the catastrophic Chiufengershan rock avalanche, and highlights the

site-specific controls of varying lithology and topography on seismic anisotropy in terms of differing landslide velocity response to earthquake triggering (Fig. 15; Dong et al., 2009).

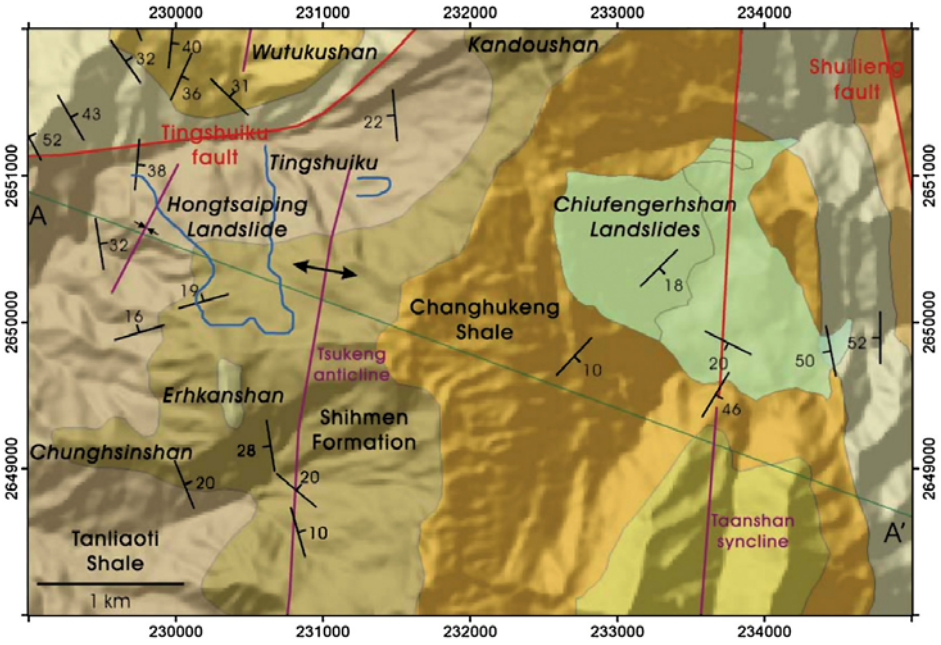

Fig. 15. Geological map of the Hongtsaiping landslide area. The area of this large slow-moving landslide is mainly at the left limb of Tsukeng Anticline, and the right limb of a small syncline. The northern landslide area is bounded by Tingshuiku Fault, whereas the detachment area of the catastrophic Chiufengershan landslide is ~2.5 km to the east (after Tseng et al., 2009).

Reactivation of former landslides is another important and often observed mechanism during strong earthquakes. For example, in the Tachia River catchment of Taiwan, the 1999 Chi-Chi earthquake is thought to have reactivated 51% of the area attributed to pre-existing slope instabilities that were triggered by rainstorms, whereas major typhoons following the earthquake had reactivated between 59% and 66% of the area of coseismic landslides (Chuang et al., 2009). This range of ratios encompasses earlier estimates in comparably affected Taiwanese river basins (e.g. Lin et al., 2008a). Similarly, Wang et al. (2007) noted that 53% of the 1212 studied coseismic landslides attributed to the 2004 Niigata earthquake, Japan, were reactivations of previously mapped slope failures. Kamp et al. (2010) noted substantial increases in both landslide numbers and landslide-affected area in the years following the 2005 Kashmir earthquake, which they largely attributed to aftershocks. The Tsaoling landslide, Taiwan, is a particularly notorious example of large-scale reactivations that led to four catastrophic and river-blocking rockslide-rock avalanches along Chingshui River (e.g. Hsu and Hsu, 2009). Between 1941 and 1999, each of these four landslides deposited between 25 and 200 × 10^6 m^3 of rock debris at more or less the same location, creating up to 200-m high natural dams that were subsequently stacked on top of each other. Two of these reactivation events were triggered by earthquakes (Fig. 16).

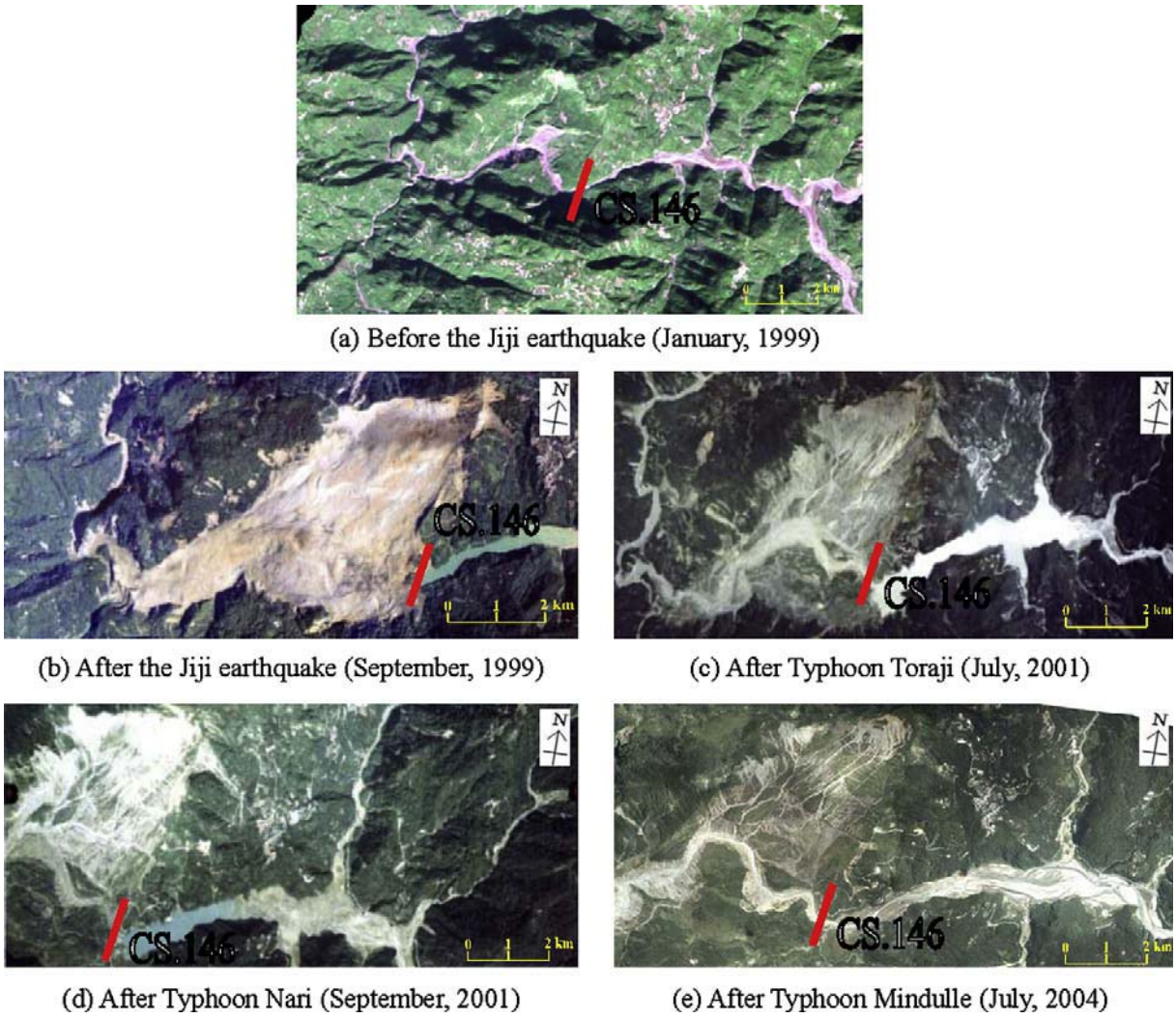

Fig. 16. Multitemporal aerial photos showing the site of Tsaoling landslide dams and the effects of landslide reactivation following earthquake and tropical cyclone disturbances (after Hsu and Hsu, 2009).

It follows that these substantial degrees of reactivation of either rainstorm-triggered landslides by earthquakes and, conversely, earthquake-triggered landslides by rainstorms has important implications for constraining and testing slope-failure susceptibility assessments. At the same time such spatial superposition of landslide locations makes it difficult to ascertain and distinguish between the eventual landslide triggers, let alone the underlying causes especially where levels of antecedent soil moisture and seismicity may vary considerably. Despite these limitations, there is preliminary evidence suggesting that the degree of landslide reactivation may be partly dependent on the experienced peak ground acceleration (Fig. 17; Chuang et al., 2009).

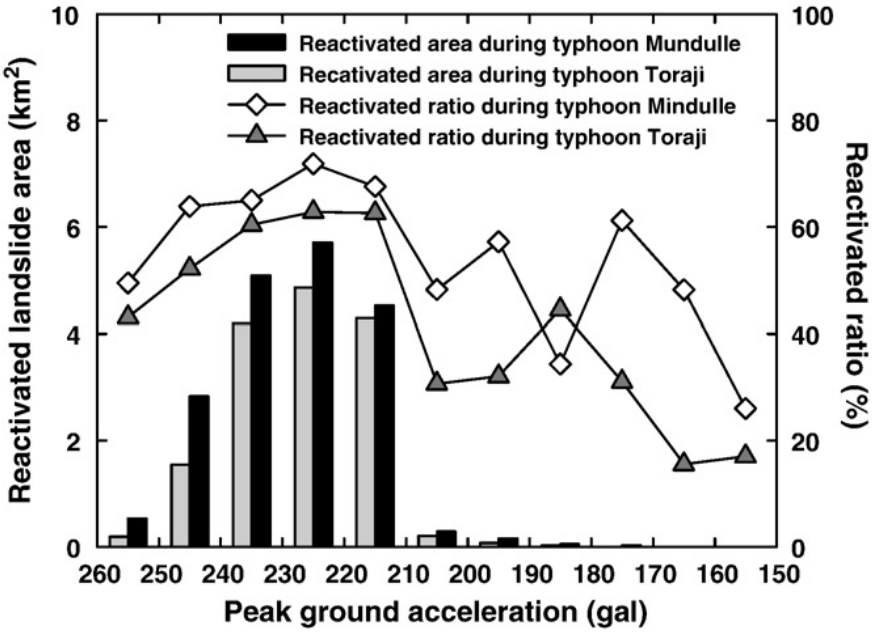

Fig. 17. The relationship between reactivated landslide area attributed to the 1999 Chi-Chi earthquake, and its peak ground acceleration, during typhoons Toraji and Mindulle. The reactivation ratio is defined as the ratio of the total area of reactivated landslides over the total landslide area triggered during an event (after Chuang et al., 2009).

5. Post-seismic landslide impacts

One of the most prominent off-site consequences of earthquake-triggered landslides that has gained much research attention over the last decade or so is the formation of large displacement waves. These waves are triggered when landslides enter water bodies or when coseismic subaquaeous landslides detach (e.g. Panizzo et al., 2005; Masson et al., 2006; Wieczorek et al., 2007; Fanetti et al., 2008; ten Brink et al., 2009; Waythomas et al., 2009). Such landslide tsunami (in marine or fjord environments) or seiches (in lakes) pose a significant hazard for near-shore environments in both coastal and alpine settings. One of the most impressive historic landslide tsunami in terms of wave height occurred during an M_w = 8.3 earthquake, south Alaska, in 1958, when a large rockslide entered the head of Lituya Bay. The landslide impact rapidly displaced coastal water masses, and created a tsunami with a runup height of 524 m, causing thorough though highly localized stripping of surficial sediments and soil cover (Fritz et al., 2009; Fig. 18). Recognising and distinguishing from the geological record the potential for such local landslide sources of tsunami from regional ones (i.e. tsunami triggered directly through seismic fault rupture) is an important task for reconstructing seismic and landslide tsunami hazard.

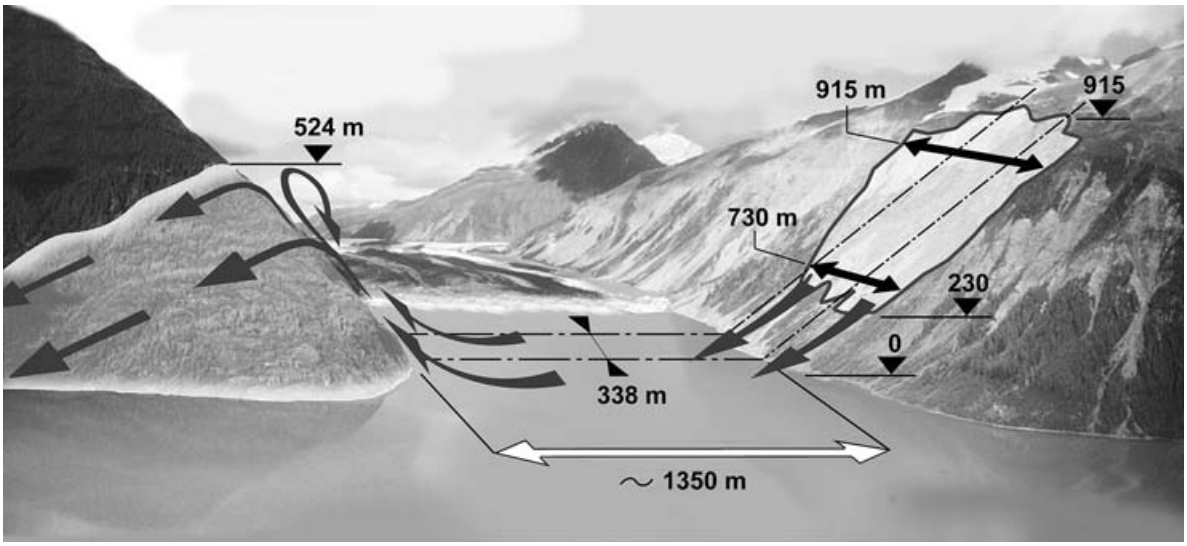

Fig. 18. Gilbert Inlet illustration showing landslide dimensions, impact site and tsunami runup to 524 m on spur ridge directly opposite to landslide impact (original motion of the landslide was from right side of picture to the left). Direction of view is north and the front of Lituya Glacier is set to 1958 post-slide position. Illustration background is synthesized from two aerial photos recorded in 1997 (Photos: courtesy of Charles L. Mader; after Fritz et al., 2009).

It has further well been recognised that earthquakes are precursors to substantial sedimentary pulses in mountain belts and their forelands (Fig. 19; e.g. Pain and Bowler, 1973; Pearce and Watson, 1986; Keefer, 1999; Dadson et al., 2004). An important aspect in this regard is the reactivation of coseismic landslides and debris flows during subsequent rainstorms. Thus the magnitude and frequency of such landscape-scale disturbance events largely governs the fate of coseismically generated landslide debris. Correspondingly, the delivery and fluvial routing of earthquake-generated debris is highly variable judging from the small, but growing, number of studies that have attempted to quantify post-earthquake sediment flux.

The spectrum of post-seismic sediment delivery of landslide debris to river channels is roughly encompassed by work on the 1970 Madang (Papua New Guinea), and the 1929 Murchison (New Zealand) earthquakes (Pain and Bowler, 1973; Pearce and Watson, 1986). In Papua New Guinea nearly half of the landslide-derived sediment had been cleared from the affected headwater catchments several years after the event. The New Zealand catchments, however, retained about half of the debris in headwaters due to large calibre and sediment trapping in several stable earthquake-triggered landslide-dammed lakes. Owen et al. (1996) estimated a post-seismic sediment delivery ratio (SDR), i.e. the fraction of sediment leaving a catchment with respect to the total generated by earthquake-triggered landslides, between 0.5 and 0.84, following the 1991 Garhwal earthquake, India. Historic SDR from single large coseismic landslides in the Southern Alps, New Zealand, have been estimated to be as low as <0.2 in the Southern Alps (Korup et al., 2004). Using fluvial sediment yield data for such estimates can be problematic, given that the bed-load fraction is

often difficult to quantify in mountain rivers. Using the infill history of check dams is one possible approach to more comprehensive post-seismic sediment budgets (e.g. Koi et al., 2008). Matsuoka et al. (2008) have used high-resolution LiDAR data to quantify the fate of earthquake-triggered landslide debris from the 2004 Niigata earthquake in a small (38 km^2) mountain catchment of Japan. They found that 19 months after the event, the SDR remained as low as ~0.2, which nevertheless led to an extreme corresponding sediment yield of ~4 × 10^4 t km^{-2} yr^{-1}.

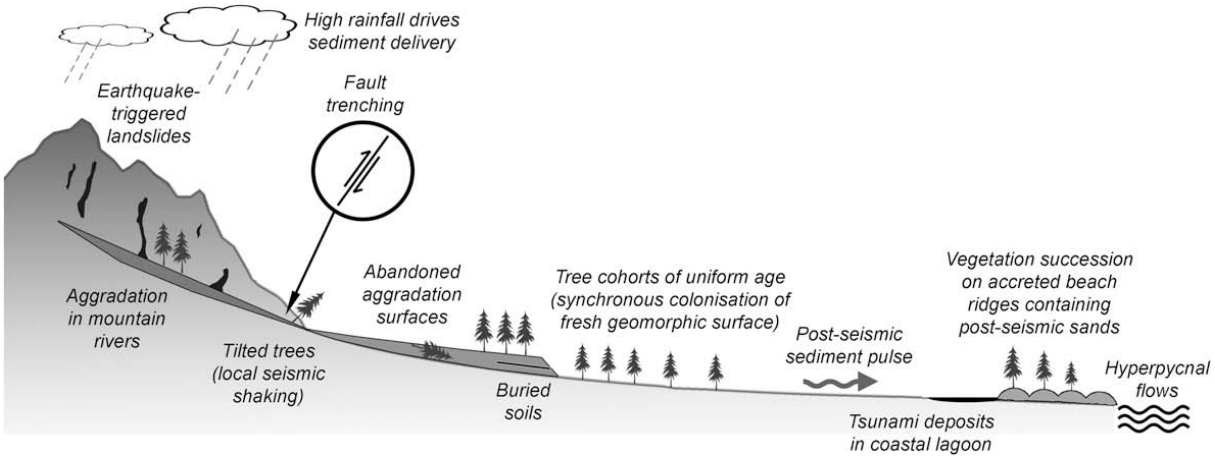

Fig. 19. Geomorphic legacy of earthquake-induced landslides and subsequent fluvial sediment pulses from the Southern Alps, New Zealand (not to scale; based on the ''seismic staircase'' model of Goff and McFadgen, 2002). Reconstructions of prehistoric earthquakes are most reliable when supported by several lines of evidence. Explosive volcanic eruptions may produce similar landform-sediment assemblages. The preservation potential of these different archives depends on the magnitude and frequency of the events that produce the sediment (after Korup and Clague, 2009).

Nevertheless, some of the most spectacular reported fluvial sediment yields documented (>10^5 t km^{-2} yr^{-1}) have occurred in the first years following regional earthquake- (e.g. Pain and Bowler, 1973; Pearce and Watson, 1986; Keefer, 1999); rainstorm-triggered landslide episodes (e.g. Page et al., 1994; Trustrum et al., 1999); or a sequence of both (e.g. Dadson et al., 2004). In Taiwan, for example, the passage of several tropical cyclones has contributed to flushing of landslide debris produced during the 1999 Chi-Chi earthquake, raising suspended sediment yields in mountain rivers to four times the background level before dropping back to normal after six years (Lin et al., 2008a, b; Fig. 20; Fig. 21).

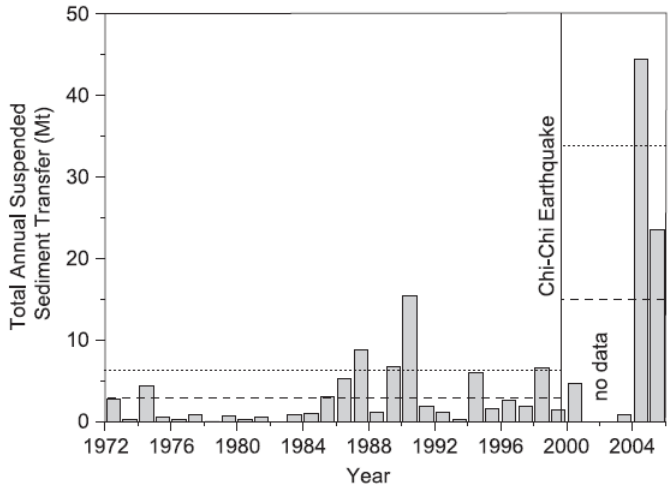

Fig. 20. Time series of total annual suspended sediment transfer at Neimaopu Station, Taiwan, from 1972 to 2005. Total annual values were calculated with a monthly weighted average method. No data are available for 2001 2002. Interannual average total annual values for intervals before and after the Chi-Chi earthquake are indicated with dashed lines, dotted lines are standard errors on these averages (after Lin et al., 2008b).

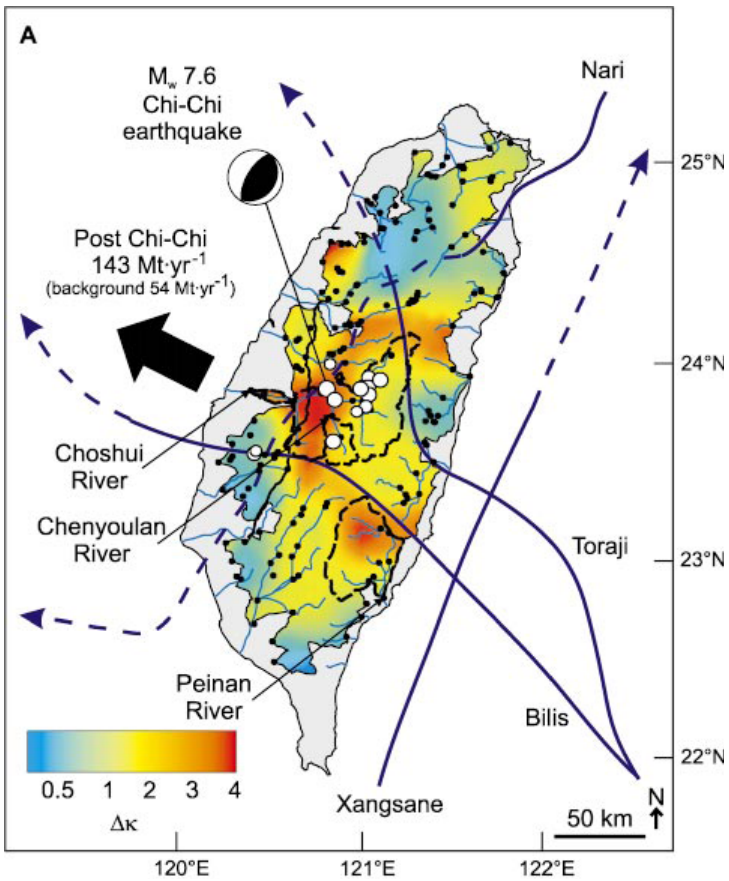

Fig. 21. Spatial variation of change in unit sediment concentration, Δκ, following Chi-Chi earthquake. Data from 101 catchments were smoothed using 30-km-diameter circular moving average. This length scale is median area of the catchments analyzed. Dashed lines show boundaries of named catchments. Black circles show gauging stations; open circles indicate Chi-Chi epicenter and aftershocks with M_L >6. Blue lines are tracks of subsequent typhoons: Bilis (average discharge at Choshui River mouth, Q_{avg} = 4850 m^3 s^{-1}), Xangsane (Q_{avg} = 1810 m^3 s^{-1}), Toraji (Q_{avg} = 7790 m^3 s^{-1}), and Nari (Q_{avg} = m^3 s^{-1}). Maximum wind velocities were 105, 74, 74, and 78 knots, respectively; track is solid if wind speed is >64 knots; dashed otherwise (after Dadson et al., 2004).

These spectacular rates are invariantly tied to humid and tectonically active mountain belts, whereas little is known about the fate of coseismic debris in more arid settings (Keefer and Mosley, 2004). Yet strong earthquakes may also promote conditions conducive to sediment storage by triggering numerous landslide-dammed lakes. For example, dry loess flows triggered by the 1920 Haiyuan earthquake (M = 8.5), China, impounded some 40 lakes (Zhang and Wang, 2007); and the 1929 Murchison earthquake (M_s = 7.7), New Zealand, was responsible for a similar number of landslide-dammed lakes, many of which have persisted until the present day (Hancox et al., 1997). The 12 May 2008 Wenchuan earthquake, Sichuan, China, formed more than 250 river-blocking landslides (Cui et al., 2009; Xu et al., 2009). Such synchronous formation of natural sediment traps further increases the potential for modulating post-seismic sediment pulses by either catastrophic sediment flushing during dam breaks (Korup and Tweed, 2007) or increasing the intermediate sediment storage capacity of valley floors by providing accommodation space in landslide-dammed lakes.

These feedbacks greatly complicate the linkage between landslide erosion and sediment delivery to river channels, as substantial fractions of the measured yields may derive from intermittent alluvial storage. Landslide-derived sediment pulses have been recorded to last for between days to several years, if not decades, depending on the definition of volumetric fraction and calibre of the sediment eventually exported from the landslide source areas (e.g. Pearce and Watson, 1986; Dadson et al., 2004; Koi et al., 2008).

Earthquake-mobilized debris provides large volumes of readily available sediment for subsequent entrainment. The flushing of material that has been stored intermittently on hillslopes into river channels causes a number of substantial geomorphic changes with potentially adverse consequences long after the causative earthquake has passed. The 2008 Wenchuan earthquake has demonstrated, however, that the most immediate hazard is posed by large river-blocking landslides that impounded large and potentially unstable water bodies (Cui et al., 2009; Xu et al., 2009; for a recent review see Korup and Tweed, 2007), inundating large tracts of valley floors and cutting off access, while threatening downstream reaches because of the potential of catastrophic dam break. Prolonged impoundment of water masses behind large natural dams further causes potential flooding and aggradation of valley floors, contaminant mobilization and concentration, deterioration of water quality, loss of aquatic habitats, and hinders access to earthquake-devastated sites (Fig. 22).

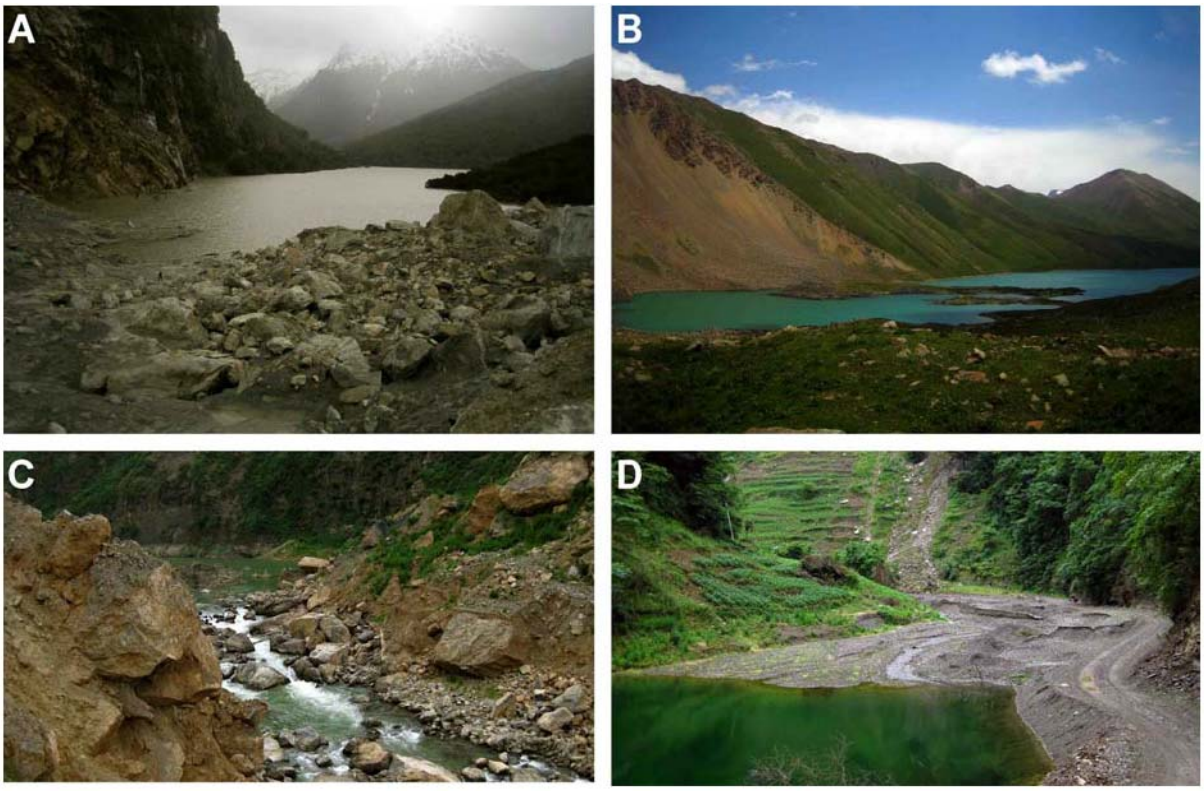

Fig. 22. Landslide dams. A. Upstream view of landslide-dammed lake, several months after its formation; Southern Alps, New Zealand. Note rounded and poorly sorted boulders in upstream dam face, resembling glacial deposits. B. Upstream view of lake dammed by at least two Holocene rock avalanches (scar mantled with scree cones); Krygyz Tien Shan. C. Upstream view of knickpoint of artificially breached landslide dam that was formed during the 2008 Wenchuan earthquake, and artificially breached shortly after; Longmen Shan, Sichuan, China. D. Upstream view of active fluvial delta front that progrades into a small landslide-dammed lake formed by the same earthquake, attesting to post-seismic increases to fluvial sediment yields; Longmen Shan, Sichuan, China.

Catastrophic outburst floods and debris flows pose substantial off-site hazards to downstream communities (see Korup and Tweed, 2007 for a recent review). Historical accounts attest to the high destruction potential of such geomorphic off-site impacts. For example, Dai et al. (2005) assert that the dam-break flood from a large earthquake-triggered (M = 7.75) landslide on the Dadu River, Sichuan, China, resulted in some 100,000 fatalities downstream in 1786. One of the most significant outburst debris flows documented in terms of extremely peaked short-term sediment yield is that following the earthquake-triggered formation of the Bairaman landslide dam, Papua New Guinea, in 1985 (King et al., 1989). During some three hours of the catastrophic dam-break process, ~80 × 10^6 m^3 were mobilized and flushed downstream in a massive debris flow that attained a flow height of ~100 m just downstream of the dam. Numerical models of flood routing demonstrate that the type of dam failure (e.g. induced by a displacement wave or breaching following overtopping) may be the prime controls on peak discharge and downstream flow stages (Risley et al., 2006; Fig. 23).

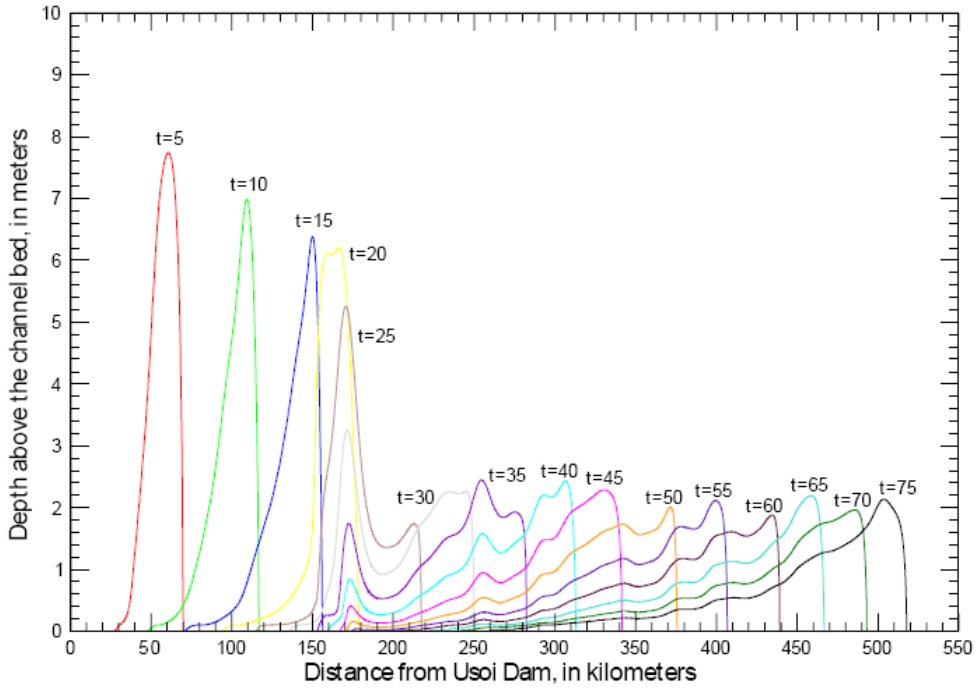

Fig. 23. Modelled flow-depth profiles for a 87 × 10^6 m^3 volume overtopping flood at landslide-dammed Lake Sarez, the world's currently highest intact natural dam (~600 m), Tajikistan, at 5-hour intervals; "t=5-75" corresponds to the number of hours after the start of the flood event for each profile. This scenario assumes a large displacement wave triggered by potential coseismic landsliding into the lake; note that after three days a flood wave >2-m high could still impact locations >500 km downstream (after Risley et al., 2006).

In addition to the geomorphic impacts of catastrophic outburst flows, sediment yields from large individual formerly river-blocking landslide deposits may significantly exceed background fluvial sediment yields, depending on the reference period. For example, fluvial dissection of the Tsaoling and Jiufengershan rock avalanches triggered by the 1999 Chi-Chi earthquake (M_w =7.6), Taiwan, produced downstream sediment yields of 1.1 to 1.8 × 10^5 m^3 km^{-2} yr^{-1}, i.e. one to two orders of magnitude higher than in undisturbed reaches, within the first years following failure (Chen et al., 2005; Chang et al., 2006). Elsewhere, fluvial dissection of deposits from single large earthquake-triggered landslides may produce sediment yields >10^4 t km^{-2} yr^{-1} in steep and small mountainous watersheds in particular (Korup et al., 2004; Korup, 2005; Mikoš et al., 2006). Moreover, comparison of worldwide examples indicates that the total amount and rate of landslide sediment delivery does not fully depend on the number of slope failures per unit study area and time. Indeed, it seems that sediment yields fed from single large landslide deposits may attain levels comparable to those of regional-scale episodes of landsliding entailing up to tens of thousands of landslides (Fig. 24).

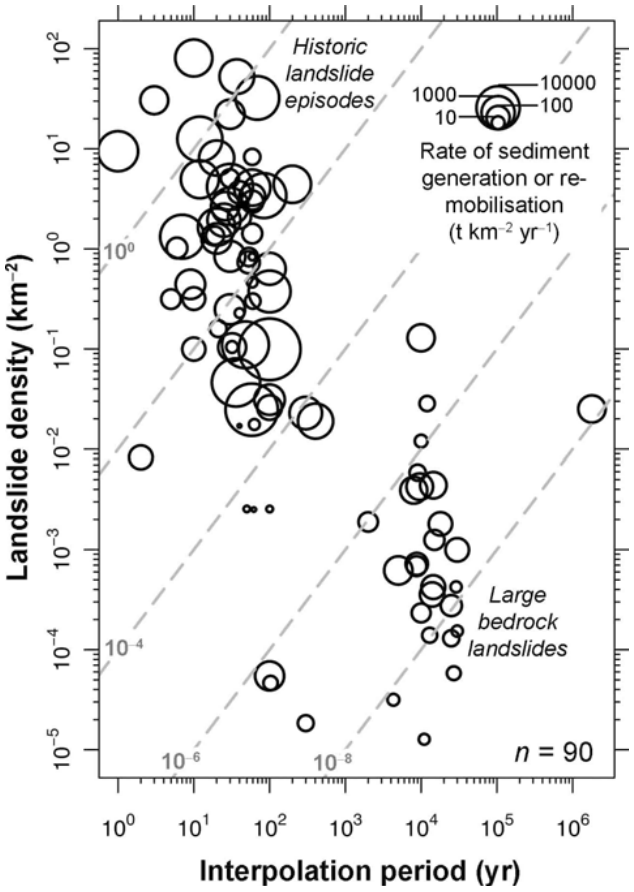

Fig. 24. Landslide density expressed as number of landslides per unit study area [km^{-2}] as a function of study interpolation period. Circle size is scaled to the rate at which landslide debris mass is generated or remobilized [t km^{-2} yr^{-1}]. Gray dashed lines denote equal landslide frequency, expressed as number of landslides per unit study area and time [km^{-2} yr^{-1}]. Historic landslide episodes triggered by earthquakes or high-intensity rainstorms achieve the highest known landslide frequencies and also some of the highest rates of landslide debris mobilization. In contrast, large bedrock landslides are orders of magnitude less frequent, by may still deliver substantial amounts of sediment to mountain rivers.

Further post-earthquake disturbance cascades are manifest in catastrophic channel changes, where sediment pulses leading to altered ambient particle size distributions, substantial channel aggradation and widening. Extremely rapid channel aggradation amounting up to 15-30 m has been documented in several steep and short mountain rivers of Taiwan, where consecutive tropical cyclones maintained flushing of coseismically and rainfall-derived landslide debris (Chen, 2009). Such catastrophic changes to channel cross sections and floodplains implicate higher flood frequencies for a given discharge regime. Additional adverse effects of landslide-derived sediment pulses involve ongoing channel instability dominated by avulsions, particularly on alluvial fans along mountain-range fronts (Korup, 2004; Davies and Korup, 2007); the destruction of aquatic habitats; and hyperpycnal flows (e.g. Kao and Milliman, 2008). In forested terrain, earthquake-induced landslides may further mobilize significant amounts of biomass, particularly large woody debris and soil organic carbon (e.g. Ren et al., 2009).

6. Conclusions

- Systematic analyses of the spatial distribution of coseismic landslides with respect to topography, lithology, anthropogenic land-use modification, and resulting seismic anisotropy have highlighted a number of distinct relationships that can be used to derive empirical envelopes to roughly predict the extent of coseismic landsliding as a function of earthquake magnitude;

- Earthquakes may trigger large, catastrophic, and highly mobile landslides such as rock avalanches in alpine glaciated terrain, and loess flows in mountainous terrain sustaining thick loess cover. Such large landslides have the highest potential for adversely interacting with the drainage network such that they may form ephemeral landslide dams subject to potential catastrophic dam break and subsequent floods and debris flows;

- Despite the substantial and geologically speaking instantaneous earthquake-induced increases to landslide numbers and fraction of terrain affected by landslides, similar degrees of regional-scale slope instability have been achieved during rainstorms or, more locally focuses, anthropogenic modification of hillslopes;

- Superposition and temporally close sequencing of earthquakes and rainstorms complicate the unambiguous identification of coseismic landslides, although there appear to be systematic differences in terms of landslide density [km^{-2}] and frequency [km^{-2} yr^{-1}] as a function of slope position and distance from the epicentre/storm centre;

- Landslide tsunami and seiches are among the most immediate subsequent hazards of earthquake-triggered landslides in mountainous terrain, particularly where Quaternary glaciations have created tall oversteepened hillslopes adjacent to deep fjords and lakes. Likewise the interference of coseismic landslides with river channels promotes the formation and potentially catastrophic failure of landslide dams, which may give rise to highly destructive outburst flows;

- Among the most common observed post-seismic effects of earthquake-triggered landslides in humid mountainous terrain is the mobilisation of significant amounts of landslide debris. The delivery of coseismic sediment to the drainage network is often

accelerated by high-intensity rainstorms, which promote extremely high and pulsed fluvial sediment yields, increases in flood frequencies, and prolonged phases of channel instability.

References

Barnard, P.L., Owen, L.A., Sharma, M.C., Finkel, R.C., 2001. Natural and human-induced landsliding in the Garhwal Himalaya of northern India. Geomorphology 40, 21-35.

Beck, C., 2009. Late Quaternary lacustrine paleo-seismic archives in north-western Alps: Examples of earthquake-origin assessment of sedimentary disturbances. Earth Science Reviews 96, 327-344.

Bommer, J.J., Rodriguez, C.E., 2002. Earthquake-induced landslides in Central America. Engineering Geology 63, 189-220.

Bourdeau, C., Havenith, H.B., 2008. Site effects modelling applied to the slope affected by the Suusamyr earthquake (Kyrgyzstan, 1992). Engineering Geology 97, 126-145.

Bull, W.B., Brandon, M.T., 1998. Lichen dating of earthquake-generated regional rockfall events, Southern Alps, New Zealand. Geological Society of America Bulletin 110, 60-84.

Bulmer, M, et al., 2007. Landslide hazards after the 2005 Kashmir earthquake. EOS, Transactions of the American Geophysical Union 88, 53-55.

Carrara, P.E., O'Neill, J.M., 2003. Tree-ring dated landslide movements and their relationship to seismic events in southwestern Montana, USA. Quaternary Research 59, 25-35.

Chang, K.J., Taboada, A., Chan, Y.C., Dominguez, S., 2006. Post-seismic surface processes in the Jiufengershan landslide area, 1999 Chi-Chi earthquake epicentral zone, Taiwan. Engineering Geology 86, 102-117.

Chen, R.F., et al., 2005. Large earthquake-triggered landslides and mountain belt erosion: the Tsaoling case, Taiwan. Comptes Rendues Geoscience 337, 1164–1172.

Chen, C.Y., 2009. Sedimentary impacts from landslides in the Tachia River Basin, Taiwan. Geomorphology 105, 355-365.

Chuang, S.C., Chen, H., Lin, G.W., Lin, C.W., Chang, C.P., 2009. Increase in basin sediment yield from landslides in storms following major seismic disturbance. Engineering Geology 103, 59-65.

Crozier, M.J., 2005. Multiple-occurrence regional landslide events in New Zealand: Hazard management issues. Landslides 2, 247-256.

Crozier, M.J., Deimel, M.S., Simon, J.S., 1995. Investigation of earthquake triggering for deep-seated landslides, Taranaki, New Zealand. Quaternary International 25, 65-73.

Cruden, D.M., Varnes, D.J., 1996. Landslide types and processes. In: Turner, A.K., Schuster, R.L. (Eds.), Landslides, Investigation and Mitigation. Special Report, vol. 247. Transportation Research Board, National Research Council, Washington, D.C., pp. 36–75.

Cui, P., Zhu, Y.Y., Han, Y.S., Chen, X.Q., Zhuang, J.Q., 2009. The 12 May Wenchuan earthquake-induced landslide lakes: distribution and preliminary risk evaluation. Landslides 6, 209-223.

Dadson, S.D., et al., 2004. Earthquake-triggered increase in sediment delivery from an active mountain belt. Geology 32, 732-736.

Dai, F.C, Lee, C.F., Deng, J.H., Tham, L.G., 2005. The 1786 earthquake-triggered landslide dam and subsequent dam-break flood on the Dadu River, southwestern China. Geomorphology 65, 205-221.

Davies, T.R.H., Korup, O., 2007. Persistent alluvial fanhead trenching resulting from large, infrequent sediment inputs. Earth Surface Processes and Landforms 32, 725-742.

Del Gaudio, V., Wasowski, J., 2007. Directivity of dynamic slope response to seismic shaking. Geophysical Research Letters 34, L12031.

Di, B., et al., 2010. Quantifying the spatial distribution of soil mass wasting processes after the 2008 earthquake in Wenchuan, China: A case study of the Longmenshan area. Remote Sensing of Environment 114, 761-771.

Dong, J.J., Lee, W.R., Lin, M.L., Huang, A.B., Lee, Y.L., 2009. Effects of seismic anisotropy and geological characteristics on the kinematics of the neighboring Jiufengershan and Hungtsaiping landslides during Chi-Chi earthquake. Engineering Geology 466, 438-457.

Evans, S.G., et al., 2009a. A re-examination of the mechanism and human impact of catastrophic mass flows originating on Nevado Huascarán, Cordillera Blanca, Peru in 1962 and 1970. Engineering Geology 108, 96-118.

Evans, S.G., et al., 2009b. Landslides triggered by the 1949 Khait earthquake, Tajikistan, and associated loss of life. Engineering Geology 109, 195-212.

Fanetti, D., Anselmetti, F.S., Chapron, E., Sturm, M., Vezzoli, L., 2008. Megaturbidite deposits in the Holocene basin fill of Lake Como (Southern Alps, Italy). Palaeogeography, Palaeoclimatology, Palaeoecology 259, 323-340.

Fritz, H.M., Mohammed, F., Yoo, J., 2009. Lituya Bay Landslide Impact Generated Mega-Tsunami 50th Anniversary. Pure and Applied Geophysics 166, 153-175.

Guzzetti, F. et al., 2009. Analysis of Ground Deformation Detected Using the SBAS-DInSAR Technique in Umbria, Central Italy. Pure and Applied Geophysics 166, 1425-1459.

Hancox, G.T., Perrin, N.D., Dellow, G.D., 1997. Earthquake-Induced landsliding in New Zealand and Implications for MM Intensity and Seismic Hazard Assessment. GNS

Client Report 43601B Prepared for Earthquake Commission Research Foundation, Lower Hutt, 85pp.

Hubbard, B., et al., 2005. Impact of a rock avalanche on a moraine-dammed proglacial lake: Laguna Safuna Alta, Cordillera Blanca, Peru. Earth Surface Processes and Landforms 30, 1251-1264.

Hsu, Y.S., Hsu, Y.H., 2009. Impact of earthquake-induced dammed lakes on channel evolution and bed mobility: Case study of the Tsaoling landslide dammed lake. Journal of Hydrology 374, 43-55.

Jibson, R.W., 1996. Use of landslides for paleoseismic analysis. Engineering Geology 43, 291-323.

Jibson, R.W., Harp, E.L., Michael, J.A., 2000. A method for producing digital probabilistic seismic landslide hazard maps. Engineering Geology 58, 271-289.

Jibson, R.W., Harp, E.L., Schulz, W., Keefer, D.K., 2006. Large rock avalanches triggered by the M 7.9 Denali Fault, Alaska, earthquake of 3 November 2002. Engineering Geology 83, 144-160.

Kamp, U., Owen, L.A., Growley, B.J., Khattak, G.A., 2010. Back analysis of landslide susceptibility zonation mapping for the 2005 Kashmir earthquake: an assessment of the reliability of susceptibility zoning maps. Natural Hazards, in press. doi:10.1007/s11069-009-9451-7.

Kao, S.J., Milliman, J.D., 2008. Water and Sediment Discharge from Small Mountainous Rivers, Taiwan: The Roles of Lithology, Episodic Events, and Human Activities. The Journal of Geology 116, 431-448.

Keefer, D.K., 1984. Landslides caused by earthquakes. Geological Society of America Bulletin 95, 406-421.

Keefer, D.K., 1994. The importance of earthquake-induced landslides to long-term slope erosion and slope-failure hazards in seismically active regions. Geology 10, 265-284.

Keefer, D.K., 1999. Earthquake-induced landslides and their effects on alluvial fans. Journal of Sedimentary Research 69, 84-104.

Keefer, D.K., 2002. Investigating landslides caused by earthquakes—a historical review. Surveys in Geophysics 23, 473-510.

Keefer, D.K., Manson, M.W., 1998. Regional distribution and characteristics of landslides generated by the earthquake. In: Keefer, D.K. (Ed.), The Loma Prieta, California, earthquake of October 17, 1989—Landslides, U.S. Geological Survey Professional Paper 1551-C, pp. 7-32.

Keefer, D.K., Moseley, M.E., 2004. Southern Peru desert shattered by the great 2001 earthquake: Implications for paleoseismic and paleo-El Niño–Southern Oscillation records. Proceedings of the National Academy of Sciences 101, 10878-10883.

Keefer, D.K., Wartman, J., Navarro Ochoa, C., Rodriguez-Marek, A., Wieczorek, G., 2006. Landslides caused by the M 7.6 Tecomán, Mexico earthquake of January 21, 2003. Engineering Geology 86, 183-197.

King, J., Loveday, I., Schuster, R.L., 1989. The 1985 Bairaman landslide dam and resulting debris flow, Papua New Guinea. Quarterly Journal of Engineering Geology 22, 257-270.

Koi, T., et al. 2008. Prolonged impact of earthquake-induced landslides on sediment yield in a mountain watershed: The Tanzawa region, Japan. Geomorphology 101, 692-702.

Korup, O., 2004. Landslide-induced river channel avulsions in mountain catchments of southwest New Zealand. Geomorphology 63, 57-80.

Korup, O., 2005. Large landslides and their effect on alpine sediment flux: South Westland, New Zealand. Earth Surface Processes and Landforms 30, 305-323.

Korup, O., Clague, J.J., 2009. Natural hazards, extreme events, and mountain topography. Quaternary Science Reviews 28, 977-990.

Korup, O., McSaveney, M.J., Davies, T.R.H., 2004. Sediment generation and delivery from large historic landslides in the Southern Alps, New Zealand. Geomorphology 61, 189-207.

Korup, O., Tweed, F., 2007. Ice, moraine, and landslide dams in mountainous terrain. Quaternary Science Reviews 26, 3406-3422.

Larsen, I.J., Montgomery, D.R., Korup, O., 2010. Landslide erosion controlled by hillslope material. Nature Geoscience, doi: 10.1038/NGEO776.

Lee, C.T., et al. 2008. Statistical approach to earthquake-induced landslide susceptibility. Engineering Geology 100, 43-58.

Lin, G.W., Chen, H., Chen, Y.H., Horng, M.J., 2008a. Influence of typhoons and earthquakes on rainfall-induced landslides and suspended sediments discharge. Engineering Geology 97, 32-41.

Lin, G.W., et al., 2008b. Effects of earthquake and cyclone sequencing on landsliding and fluvial sediment transfer in a mountain catchment. Earth Surface Processes and Landforms 33, 1354-1373.

Lin, W.T., Lin, C.Y., Chou, W.C., 2006. Assessment of vegetation recovery and soil erosion at landslides caused by a catastrophic earthquake: A case study in Central Taiwan. Ecological Engineering 28, 79-89.

Malamud, B.D., Turcotte, D.L., Guzzetti, F., Reichenbach, P., 2004. Landslides, earthquakes and erosion. Earth and Planetary Science Letters 229, 45-59.

Marano, K.D, Wald, D.J., Allen, T.I., 2010. Global earthquake casualties due to secondary effects: a quantitative analysis for improving rapid loss analyses. Natural Hazards 52, 319-328.

Masson, D.G., Harbitz, C.B., Wynn, R.B., Pedersen, G., Løvholt, F., 2006. Submarine landslides: Processes, triggers and hazard prediction. Philosophical Transactions of the Royal Society A 364, 2009-2039.

Matsuoka, A., Yamakoshi, T., Tamura, K., Maruyama, J., Ogawa, K., 2008. Sediment yield from seismically-disturbed mountainous watersheds revealed by multi-temporal aerial LiDAR surveys. IAHS-AISH Publication 325, 208-216.

Meunier, P., Hovius, N., Haines, J.A., 2007. Regional patterns of earthquake-triggered landslides and their relation to ground motion. Geophysical Research Letters 34, L20408.

Meunier, P., Hovius, N., Haines, J.A., 2008. Topographic site effects and the location of earthquake induced landslides. Earth and Planetary Science Letters 275, 221-232.

Mikoš, M., Fazarinc, R., Ribičič, N., 2006. Sediment production and delivery from recent large landslides and earthquake-induced rock falls in the Upper Soča River Valley, Slovenia. Engineering Geology 86, 198-210.

Miles, S.B., Keefer, D.K., 2009. Evaluation of CAMEL — comprehensive areal model of earthquake-induced landslides. Engineering Geology 104, 1-15.

Owen LA, Sharma MC, Bigwood R. 1996. Landscape modification and geomorphological consequences of the 20th October 1991 earthquake and the July–August 1992 monsoon in the Garhwal Himalaya. Zeitschrift für Geomorphologie Supplementband NF 103, 359-372.

Owen, L.A., et al., 2008. Landslides triggered by the 8 October 2005 Kashmir earthquake. Geomorphology 94, 1-9.

Page, M.J., Trustrum, N.A., Dymond, J., 1994. Sediment budget to assess the geomorphic effect of a cyclonic storm, New Zealand. Geomorphology 9, 169-188.

Pain, C.F., Bowler, J.M., 1973. Denudation following the November 1970 earthquake at Madang, Papua New Guinea. Zeitschrift für Geomorphologie Supplementband N.F. 18, 92-104.

Panizzo, A., De Girolamo, P., Petaccia, A., 2005. Forecasting impulse waves generated by subaerial landslides. Journal of Geophysical Research C 110, C12025.

Pearce, A.J., O'Loughlin, C.L., 1985. Landsliding during a M 7.7 earthquake: Influence of geology and topography. Geology 13, 855-858.

Pearce, A.J., Watson, A.J., 1986. Effects of earthquake-induced landslides on sediment budget and transport over a 50-yr period. Geology 14, 52-55.

Ren, D., et al., 2009. Mudslide-caused ecosystem degradation following Wenchuan earthquake 2008. Geophysical Research Letters 36, L05401.

Risley, J., Walder, J., Denlinger, R., 2006. Usoi dam wave overtopping and flood routing in the Bartang and Panj Rivers, Tajikistan. U.S. Geological Survey Water-Resources Investigations Report 03-4004, 37pp.

Rodriguéz, C.E., Bommer, J.J., Chandler, R.J., 1999. Earthquake-induced landslides: 1980–1997. Soil Dynamics and Earthquake Engineering 18, 325-346.

Sato, H.P. et al., 2007. Interpretation of landslide distribution triggered by the 2005 Northern Pakistan earthquake using SPOT 5 imagery. Landslides 4, 113-122.

Saygili, S., Rathje, E.M., 2009. Probabilistically based seismic landslide hazard maps: An application in Southern California. Engineering Geology 109, 183-194.

Schuster, R.L., Alford, D., 2004. Usoi landslide dam and Lake Sarez, Pamir Mountains, Tajikistan. Environmental and Engineering Geoscience 10, 151-168.

Schuster, R., Logan, R., Pringle, P., 1992. Prehistoric rock avalanches in the Olympic Mountains, Washington. Science 258, 1620-1621.

Sidle, R.C., Ochiai, H., 2006. Landslides. Processes, Prediction, and Land Use. AGU Water Resources Monograph 18, 312pp.

ten Brink, U.S., Lee, H.J., Geist, E.L., Twichell, D., 2009. Assessment of tsunami hazard to the U.S. East Coast using relationships between submarine landslides and earthquakes. Marine Geology 264, 65-73.

Thapa, G.B., Paudel, G.S., 2002. Farmland degradation in the mountains of Nepal: a study of watersheds ‘with’ and ‘without’ external intervention. Land Degradation and Development 13, 479-493.

Trustrum, N.A., Gomez, B., Page, M.J., Reid, L.M., Hicks, D.M., 1999. Sediment production, storage and output: The relative role of large magnitude events in steepland catchments. Zeitschrift für Geomorphologie NF 115, 71-86.

Tseng, C.H., et al., 2009. Non-catastrophic landslides induced by the M_w 7.6 Chi-Chi earthquake in central Taiwan as revealed by PIV analysis. Tectonophysics 466, 427-437.

Wang, H.B., Sassa, K., Xu, W.Y., 2007. Analysis of a spatial distribution of landslides triggered by the 2004 Chuetsu earthquakes of Niigata Prefecture, Japan. Natural Hazards 41, 43-60.

Waythomas, C.F., Watts, P., Shi, F., Kirby, J.T., 2009. Pacific Basin tsunami hazards associated with mass flows in the Aleutian arc of Alaska. Quaternary Science Reviews 28, 1006-1019.

Wieczorek, G.F., Geist, E.L., Motyka, R.J., Jakob, M., 2007. Hazard assessment of the Tidal Inlet landslide and potential subsequent tsunami, Glacier Bay National Park, Alaska. Landslides 4, 205-215.

Witham, C.S., 2005. Volcanic disasters and incidents: a new database. Journal of Volcanology and Geothermal Research 148, 191-233.

Xu, Q., Fan, X.-M., Huang, R.-Q., Van Westen, C., 2009. Landslide dams triggered by the Wenchuan Earthquake, Sichuan Province, south west China. Bulletin of Engineering Geology and the Environment 68, 373-386.

Yagi, H., Sato, G., Hikagi, D., Yamamoto, M., Yamasaki, T., 2009. Distribution and characteristics of landslides induced by the Iwate-Miyagi Nairiku Earthquake in 2008 in Tohoku District, Northeast Japan. Landslides 6, 335-344.

Yamagishi, H., Iwahashi, J., 2007. Comparison between the two triggered landslides in Mid-Niigata, Japan by July 13 heavy rainfall and October 23 intensive earthquakes in 2004. Landslides 4, 389-387.

Yin, J., Chen, J., Xu, X.W., Wang, X., Zheng, Y., 2010. The characteristics of the landslides triggered by the Wenchuan Ms 8.0 earthquake from Anxian to Beichuan. Journal of Asian Earth Sciences 37, 452-459.

Zhang, D., Wang, G., 2007. Study of the 1920 Haiyuan earthquake-induced landslides in loess (China). Engineering Geology 94, 76-88.